Nonlinear Dyn
https://doi.org/10.1007/s11071-020-05908-9

ORIGINAL PAPER

Nonlinear mode coupling in a passively isolated mechanical system

Sunit K. Gupta · Mohammad A. Bukhari · Oumar R. Barry

Received: 23 December 2019 / Accepted: 20 August 2020

Abstract Recent studies in passively isolated systems have shown that mode coupling is desirable for better vibration suppression, thus refuting the long-standing rule of modal decoupling. However, these studies have ignored the nonlinearities in the isolators. In this work, we consider stiffness nonlinearity from pneumatic isolators and study the nonlinear forced damped vibrations of a passively isolated ultra-precision manufacturing (UPM) machine. Experimental analysis is conducted to guide the mathematical formulation. The system comprises linearly and nonlinearly coupled in-plane horizontal and rotational motion of the UPM machine with quadratic nonlinear stiffness from the isolators. We present an analytical study using the method of multiple scales and the method of harmonic balance for different cases of external resonances, viz., the primary and the secondary resonances (superharmonic and combined resonances) with 1 : 2 internal resonance between the modes. We further validate our analytical findings using direct numerical integration and observe an excellent match. On extending our analysis, we observe the existence of subcritical, supercritical, and *s*-shaped bifurcation depending on the location of the isolators and the case of external resonance. Also, the saturation and quasi-saturation phenomenon are observed for the case of resonances close to the higher natural frequency and combined resonance, respectively. A parametric study is conducted to examine the effect of different parameters on the dynamics of the system, and consecutively the critical parameters of the system are identified for different cases of external resonance.

Keywords Ultra-precision manufacturing machine · Mode-coupling · saturation · Quasi-saturation · s-shaped bifurcation · Subcritical and supercritical bifurcation · Internal · Primary · Superharmonic, Combined resonance

1 Introduction

Over the last few years, the use of machine parts with micro-level patterns and nano-level surface finish has been significantly increased in the electronic, biomedical, and communication industries [1–3]. To meet the stringent requirements at the microscale, ultra-precision manufacturing (UPM) machines like ultra-precision machine tools, water scanners, and micro-coordinate measuring machine (CMM) are used to manufacture or measure these parts. As the tolerance and accuracy of these parts are very high, even the smallest amplitude of vibrations can adversely affect the accuracy and precision of the UPM machine. Therefore, it is required to understand the dynamics of such precision equipment under the influence of external excitations. This is the focus of the current work.

Vibration isolation of a mechanical system from its surroundings can be achieved by interposing an isola-

S. K. Gupta · M. A. Bukhari · O. R. Barry (✉)
Department of Mechanical Engineering, Virginia Tech, Blacksburg, VA 24061, USA
e-mail: obarry@vt.edu

Published online: 02 September 2020

tion mount between the source of the excitation and the system. These isolation mounts can be passive, active, or semi-active [4–9]. However, the use of passive isolators in engineering applications is more popular as compared to active, and semi-active because of their cost-effectiveness, reliability, and simple installation [10–12]. The basic principle of efficient passive isolation relies on making the foundation of the system so flexible that the natural frequencies of the system become small (sufficiently far from the external excitation frequencies) to avoid resonance [13–15]. Then, based on the linear theory of vibration isolation [16–18], the system is considered to be adequately isolated. On the other hand, the use of low stiffness passive isolators in UPM machines causes the emergence of residual vibrations in the form of low-frequency rocking motions due to an internal or external excitation [19]. Therefore, to maintain the accuracy of these systems, these residual vibrations must be minimized [10,11,20,21]. Another drawback of passive isolators with the viscously damped oscillators is the increased transmissibility at frequencies higher than resonance frequencies [6,10,20]. These two drawbacks of passive isolators can be avoided using pneumatic isolators (i.e., nonlinear vibration isolators) [19,22–27]. We emphasize that inclusion of nonlinearity in practical isolators has been well-established in the literature [28–30]. However, the inclusion of these nonlinearities in isolators causes the emergence of primary and secondary resonance, complex motions, and coupling between different modes. Another critical factor in designing these pneumatic isolators is the selection of the isolator location in such a way that mode coupling can be avoided [11]. It was observed that the decoupling between the modes could be achieved by aligning the isolator location with the center of gravity (C.G.) of the UPM machine [20,31,32]. The decoupling between the modes restricts the transmission of vertical ground motion to the horizontal axis and hence rocking motion of UPM [11,21]. Also, the decoupling between modes avoids the presence of other peaks in the transmissibility response of the machine [33].

In an attempt to explore the dynamics of UPM with coupled modes, a mathematical model with linear mode coupling between the translational and rocking motion (via the location of isolators) was first developed by Okwudire [22,34,35]. It was shown that coupling between the translational and rocking motion is desirable to minimize residual vibrations. Accordingly, the optimum value of the isolator location from the C.G. of the UPM machine is obtained [22]. Furthermore, it was observed that with this optimum value of isolator location, fivefold reduction in the vibration amplitude could be achieved with proportional damping. Later on, Lee and Okwudire [35] investigated the effect of mode coupling on the residual vibration with non-proportional damping in the system and observed that though non-proportional damping changes the behavior of the system. it still provides a significant reduction in the vibration amplitude. These findings refuted the long-standing rule of thumb that modal decoupling, rather than mode coupling, was preferable for vibration reduction in UPM machines. However, we emphasize that in Okwudire's work [22,34,35], the nonlinear stiffness of the pneumatic isolators was not considered—which is more realistic than linear stiffness. Therefore, the effect of nonlinear pneumatic isolators on the dynamics of UPM machines was not explored.

Note that the nonlinear vibration analysis of dynamical systems with coupled modes is well studied in the literature [36–40]. For instance, the effect of nonlinear mode coupling in multiple-degree-of-freedom system was studied through nonlinear damping [41] or nonlinear stiffness [40] or the combination of both [39]. It was observed that in the presence of internal resonance (depending on the nature of nonlinearity in the system) [39,40], the nonlinear mode coupling enhances energy dissipation and hence effective reduction in vibration. We emphasize that although the benefits of nonlinear mode coupling on the energy dissipation are well established, to the best of our knowledge, the effect of nonlinear mode coupling on the vibration isolation of UPM has not been explored yet. We also emphasize that there is no study that examines the interplay between nonlinear mode coupling, isolator location, and bifurcation in an isolated mechanical system. The present study aims to address this knowledge gap. Unlike in Okwudire's work [22,34], here we consider the nonlinearity in the stiffness of the pneumatic isolators and study the nonlinear dynamics of a passively isolated UPM machine under primary and secondary resonances. Experiments are carried out to guide the mathematical formulation. The exact coupled nonlinear equations of motion of the isolated machine are presented, and the analytical solutions are obtained using the method of multiple scales. The analytical results are verified against the numerical simulations for different cases of external resonance with $1:2$ internal resonance. The existence and stabil-

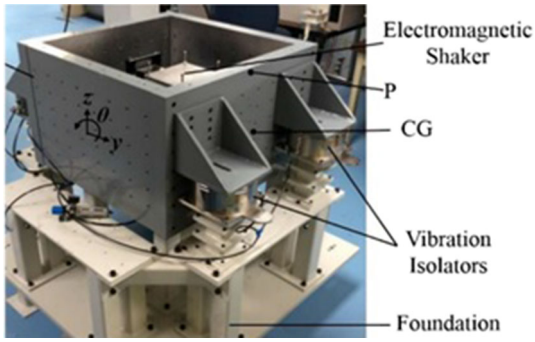

Fig. 1 Experimental setup [35]

ity of all possible steady states for the different cases of resonance are presented. Also, a parametric study is conducted to identify the critical system parameters. The rest of the paper is organized as follows. Some experimental results are presented in Sect. 2 decides the nature of nonlinearity in the system. In Sect. 3, we outline the mathematical model of the UPM machine employed for the analysis. The nonlinear analysis of this model using the method of multiple scales (MMS) for primary and secondary resonance is presented in Sect. 4. In Sect. 5, we validate the analytical results from MMS with numerical simulations and further present the nonlinear characteristic of the system. In an attempt to find key system parameters, the effect of different system parameters on the system dynamics is presented in Sect. 6. Finally, some conclusions are drawn in Sect. 7.

2 Experimental results

Experiments are carried out using the reconfigurable UPM machine prototype depicted in Fig. 1 [35]. The prototype consists of an 800 kg base of dimensions $749.3 \times 749.3 \times 495.3$ mm. The machine is supported by four pneumatic isolators (Bilz model BiAir 1-ED). The UPM machine is disturbed with initial displacements in the y-direction, and the vibration of the system is measured using a triaxial accelerometer (PCB Piezotronics model Y356A63) with sensitivity of 10.58 mV/g. The experimental results show that the prototype machine can exhibit either stable or unstable motion depending on the applied initial displacement. A very low initial disturbance yields a stable vibration motion, while a relatively larger displacement exhibits an unstable motion.

Figure 2a shows the experimental time response of the vibrating UPM machine in all three directions. The instability can be observed in all directions; however, higher vibration amplitudes occur in the y- and z-directions. This is expected as the system is disturbed in the y-direction, resulting in coupling in the y–z plane. The zoomed windows indicate the existence of multiple frequency components in each measured direction. These components represent the natural frequencies of the system along with nonlinear frequency components. For results in the x-direction (i.e., the system was not excited in this direction), we observe high noise-to-signal ratio. Therefore, we apply low-pass filter to keep the lowest dominant frequency components and eliminate noise associated with high frequency. The filtered signal is shown in the solid black curve. To further analyze the system and response frequency content, we plot the fast Fourier transform of the time responses in all measured directions as shown in Figs. 2b–2d. In Fig. 2b, it is observed that the signal in the y-direction has three dominant frequency components 1.56, 3.12, and 4.68 Hz. The first one has the highest amplitude and represents the frequency in this direction. Note that the fundamental frequency of the UPM machine is nearly half of the second mode, which corresponds to subharmonic resonance. This observation suggests that the stiffness of the pneumatic isolator is of a quadratic nonlinear type, thus confirming the type of nonlinearity of the pneumatic isolator mentioned in the literature [42]. The observed secondary resonance can further be demonstrated by plotting the response in the other coupled direction as shown in Fig. 2c. The results in z-direction indicate that the system has two coupled modes 1.56, 4.68 Hz with other smaller components representing the secondary resonances. Finally, the frequency response for the x-direction is shown in Fig. 2d. The results indicate that the magnitude of the frequency components is much lower as compared to other directions. This is not surprising since the system was not excited in this direction. Indeed, the appearance of this component in this direction might be caused by nonlinear interaction. In addition, we observe a frequency component at 3.5 Hz. This component corresponds to the unexcited mode of the machine. Indeed, this mode is also shown in Figs. 2b–2c with much smaller components.

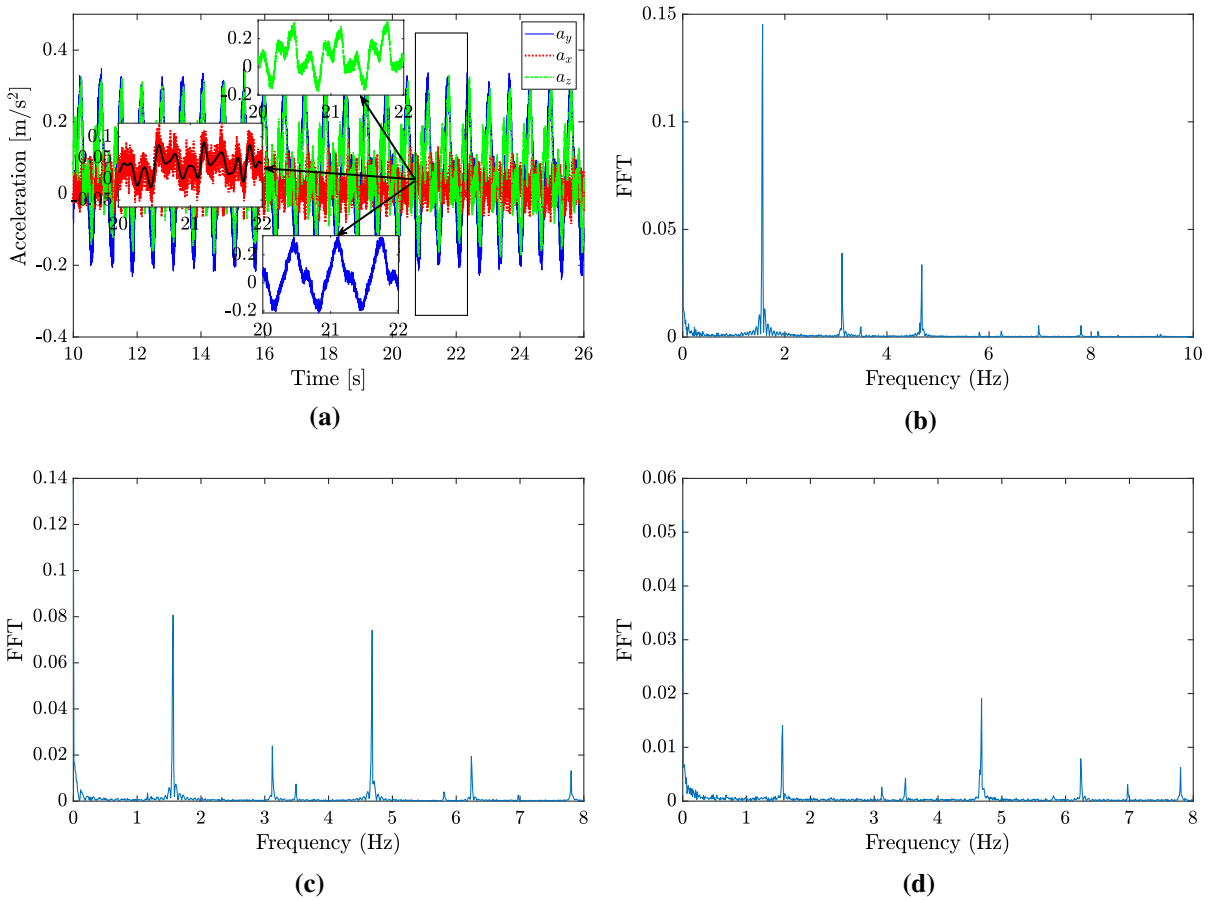

Fig. 2 Experimental results showing **a** time response; **b** frequency content of measurement in y-direction; **c** frequency content of measurement in z-direction; and **d** frequency content of measurement in x-direction

3 Mathematical model

In this section, we briefly outline the mathematical model for the UPM machine considered in this work. A schematic of the 2D-model of a UPM with pneumatic isolators is shown in Fig. 3 [35]. It consists of UPM as a rigid body with a mass m and moment of inertia I, which can translate in the y-direction and rotate in the y-z plane. Further, UPM rests on two identical pneumatic isolators. These isolators are modeled as spring-damper systems with k_y, q_y, and C_y as combined linear stiffness, quadratic stiffness, and damping coefficient, respectively, in the y-direction. k_z, q_z, and C_z are combined linear stiffness, quadratic stiffness, and damping coefficient, respectively, in the z-direction. h and b represent the distance of the isolators from the centroid (C.G.) in vertical and horizontal directions, respectively. In the current work, disturbances from surroundings are modeled as a harmonic excitation with amplitude F_0 and frequency ω_0. For the sake of simplicity, we assume that the force is acting in the y-direction at the location of the horizontal (y-direction) isolator. If y and θ_x represent the translational and rocking motion of the UPM machine, then the governing equations of motions are

$$m\ddot{y} + C_y\left(\dot{y} - h\cos\theta_x\dot{\theta}_x\right) + k_y\ (y - h\sin\theta_x) + q_y\ (y - h\sin\theta_x)^2 = F_0\ \cos\left(\omega_0\, t\right)\ , \tag{1a}$$

$$I\ddot{\theta}_x + C_z b^2\cos\theta_x\dot{\theta}_x - C_y h\left(\dot{y} - h\cos\theta_x\dot{\theta}_x\right) + b^2 k_z\sin\theta_x + b^3 q_z\sin\theta_x^2 - q_y\, h\,(y - h\sin\theta_x)^2 - k_y\, h\,(y - h\sin\theta_x) = -F_0\ \cos\left(\omega_0 t\right) h\ . \tag{1b}$$

For small amplitudes of y and θ_x, the above equations of motion can be rewritten as

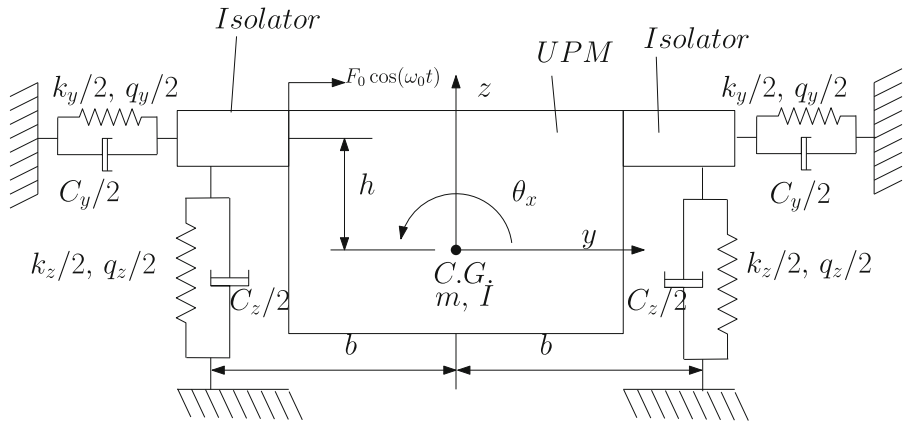

Fig. 3 Schematic of UPM with isolators with quadratic nonlinearity

$$m\ddot{y} + C_y\left(\dot{y} - h\dot{\theta}_x\right) + k_y(y - h\theta_x) + q_y(y - h\theta_x)^2 = F_0\cos(\omega_0 t)\,, \tag{2a}$$

$$I\ddot{\theta}_x + C_z b^2\dot{\theta}_x - C_y h\left(\dot{y} - h\dot{\theta}_x\right) + k_\theta\theta_x + q_\theta\theta_x^2 - q_y h(y - h\theta_x)^2 - k_y h(y - h\theta_x) = -F_0\cos(\omega_0 t)h. \tag{2b}$$

with $k_\theta = b^2 k_z$ and $q_\theta = b^3 q_z$. The above equations describe the evolution of the two coupled modes, i.e., y and θ_x with time under the effect of external harmonic excitation. It is to be noted here that both modes of UPM are linearly and nonlinearly coupled through the location of isolator in the y-direction and will be completely independent to each other if isolators are aligned with the C.G. of the UPM. We nondimensionalize the equations of motion to reduce the effective number of parameters to further ease the analysis. For this purpose, we use the following nondimensional scales and parameters:

$$\tilde{t} = t\sqrt{\frac{k_\theta}{I}},\ \hat{\zeta} = \frac{C_y}{2\sqrt{k_y m}},\ \hat{\kappa} = \frac{C_z b^2}{2\sqrt{I k_\theta}},\ \beta = \frac{\sqrt{\frac{k_y}{m}}}{\sqrt{\frac{k_\theta}{I}}},\ \alpha_1 = \frac{q_y b^3}{k_\theta},\ m_r = \frac{I}{mb^2},\ \alpha = \frac{h}{b},\ \bar{f}_0 = \frac{F_0}{bk_z},\ \omega_r = \frac{\omega_0}{\sqrt{\frac{k_\theta}{I}}},$$

$$q_{zr} = \frac{q_\theta}{k_\theta},\ k_r = \frac{k_y b^2}{k_\theta},\ \tilde{y} = \frac{y}{b}\,. \tag{3}$$

Using the aforementioned nondimensional scales and parameters, equations of motion (Eq. (2)) can be nondimensionalized as

$$\ddot{\tilde{y}} + 2\hat{\zeta}\beta\left(\dot{\tilde{y}} - \alpha\dot{\theta}_x\right) + \beta^2(\tilde{y} - \alpha\theta_x) + \alpha_1 m_r(\tilde{y} - \alpha\theta_x)^2 = \bar{f}_0 m_r\cos\left(\omega_r\tilde{t}\right)\,, \tag{4a}$$

$$\ddot{\theta}_x + 2\hat{\kappa}\dot{\theta}_x - 2\hat{\zeta}\sqrt{\frac{k_r}{m_r}}\alpha\left(\dot{\tilde{y}} - \alpha\dot{\theta}_x\right) + \theta_x + q_{zr}\theta_x^2 - \alpha_1\alpha(\tilde{y} - \alpha\theta_x)^2 - k_r\alpha(\tilde{y} - \alpha\theta_x) = -\bar{f}_0\alpha\cos\left(\omega_r\tilde{t}\right)\,, \tag{4b}$$

where $(\dot{})$ represents the derivative with respect to $\tilde{t}$, $\hat{\zeta}$ and $\hat{\kappa}$ are the damping ratio in the translational and rocking directions, respectively, β is the ratio of the natural frequencies corresponding to the uncoupled translational and rocking motions, m_r is the inertia ratio, α_1 and q_{zr} are the nondimensional quadratic stiffness in translational and rocking directions, respectively, k_r is the ratio of linear stiffnesses of equivalent isolators in translational and rocking directions, α is the nondimensional location of the isolators, f_0 is the nondimensional excitation amplitude, and ω_r is the nondimensional excitation frequency. For notational convenience, we drop the tilde and subscript x and rewrite Eq. (4) as

$$\ddot{y} + 2\,\hat{\zeta}\,\beta\,\left(\dot{y} - \alpha\,\dot{\theta}\right) + \beta^2\,(y - \alpha\,\theta) + \alpha_1\,m_r\,(y - \alpha\,\theta)^2 = \bar{f}_0\,m_r\,\cos\left(\omega_r\,t\right)\,, \tag{5a}$$

$$\ddot{\theta} + 2\hat{\kappa}\dot{\theta} + \theta + q_{zr}\theta^2$$

$$-2\hat{\zeta}\sqrt{\frac{k_r}{m_r}}\alpha\left(\dot{y}-\alpha\dot{\theta}\right)-\alpha_1\,\alpha\,(y-\alpha\,\theta)^2$$
$$-k_r\,\alpha\,(y-\alpha\,\theta)=-\bar{f}_0\,\alpha\,\cos(\omega_r\,t)\,. \tag{5b}$$

Equations (5a) and (5b) represent the nondimensional equations of motion in translational and rocking directions, respectively.

4 Perturbation analysis

As mentioned earlier, our prime interest in this work is to understand the effect of mode coupling on the nonlinear dynamics of the system, which further requires the exact solution of the system of equations (Eq. (5)). Note that the equations of motion governing the dynamics of the system (Eq. (5)) involve nonlinear quadratic terms, and it is difficult to obtain the exact solution for such systems. However, for small values of nonlinear quadratic stiffness, the approximate solution may be obtained using existing perturbation methods. With the same motivation, we use the method of multiple scales (MMS) in particular to obtain the approximate solution of the system. For this purpose, we follow the procedure outlined in [43] and introduce a small dimensionless parameter ϵ ($\epsilon \ll 1$) in the governing equations through rescaling

$$y(t)=\epsilon\eta(t)\,,\,\theta(t)=\epsilon\vartheta(t)\,. \tag{6}$$

We also rescale the damping coefficients such that the effect of damping and nonlinearity appears in the same order of ϵ. Therefore, we let $\hat{\zeta}=\epsilon\zeta$ and $\hat{\kappa}=\epsilon\kappa$. Substitution of these scalings in Eq. (5) leads to

$$\ddot{\eta}+2\epsilon\zeta\beta\left(\dot{\eta}-\alpha\dot{\vartheta}\right)+\beta^2\left(\eta-\alpha\vartheta\right)$$
$$+\epsilon\alpha_1 m_r\,(\eta-\alpha\vartheta)^2=\frac{\bar{f}_0}{\epsilon}m_r\cos(\omega_r t)\,, \tag{7a}$$

$$\ddot{\vartheta}+2\epsilon\kappa\dot{\vartheta}-2\epsilon\zeta\sqrt{\frac{k_r}{m_r}}\alpha\left(\dot{y}-\alpha\dot{\vartheta}\right)+\vartheta$$
$$+\epsilon q_{zr}\vartheta^2-\epsilon\alpha_1\alpha\,(y-\alpha\vartheta)^2$$
$$-k_r\alpha\,(y-\alpha\vartheta)=-\frac{\bar{f}_0}{\epsilon}\alpha\cos(\omega_r t)\,. \tag{7b}$$

It is noteworthy here that after substitution of scalings, we have already divided the equations throughout ϵ to get the above equation (Eq. (7)). Since the nonlinear and damping terms appear at $\mathcal{O}(\epsilon)$, the system becomes a weakly nonlinear system and can be solved using MMS. Having obtained the perturbed equations, now we present the linear and nonlinear analysis of the system in the subsequent sections.

4.1 Linear analysis

In this section, the linear analysis of the nonlinear system given by Eq. (7) is presented. This linear analysis provides the solution to the unperturbed linear equation without forcing, which will be further used to build up a solution for the perturbed nonlinear equation (Eq. (7)). The linearized coupled system of equation without forcing can be obtained by setting $\epsilon=0$ and $f_0=0$ in Eq. (7) to obtain

$$\ddot{\eta}+\beta^2\left(\eta-\alpha\,\vartheta\right)=0\,, \tag{8a}$$
$$\ddot{\vartheta}+\vartheta-k_r\,\alpha\,(y-\alpha\,\vartheta)=0\,. \tag{8b}$$

To obtain the characteristic equation, we substitute $\eta(t)=\eta_0 e^{\lambda t}$ and $\vartheta=\vartheta_0 e^{\lambda t}$ in Eq. (8) to obtain

$$\lambda^2\eta_0+\beta^2\left(\eta_0-\alpha\,\vartheta_0\right)=0\,, \tag{9a}$$
$$\lambda^2\vartheta_0+\vartheta_0-k_r\,\alpha\,(\eta_0-\alpha\,\vartheta_0)=0\,. \tag{9b}$$

Note that, for the nontrivial solutions of η_0 and ϑ_0, the determinant of the coefficient matrix of the above system must vanish. This solvability condition further leads to the characteristic equation as

$$\lambda^4+\left(1+k_r\alpha^2+\beta^2\right)\lambda^2+\beta^2=0\,. \tag{10}$$

Further, to obtain the natural frequencies of the system, we set $\lambda=i\omega$ in Eq. (10) and solve for ω to get $\omega_1=\frac{\sqrt{A+B}}{2}$, $\omega_2=\frac{\sqrt{A-B}}{2}$, where $A=2+2\,k_r\,\alpha^2+2\,\beta^2$ and $B=\sqrt{A^2-16\beta^2}$ which further implies $\omega_1>\omega_2$. Accordingly, the solution of the coupled linearized system without forcing can be written as

$$y(t)=A_1\mathbf{r_1}e^{i\omega_1 t}+A_2\mathbf{r_2}e^{i\omega_2 t}+C.C.\,, \tag{11}$$

where $y(t)=[\eta(t),\vartheta(t)]^T$, A_1, A_2 are arbitrary constants with $\mathbf{r_1}$ and $\mathbf{r_2}$ as the generalized right eigenvectors corresponding to the eigenvalues $\lambda=i\omega_1$ and $\lambda=i\omega_2$, respectively. For our system, $\mathbf{r_1}$ and $\mathbf{r_2}$ are

$$\mathbf{r_1}=\begin{bmatrix}\Lambda_1\\1\end{bmatrix},\quad \mathbf{r_2}=\begin{bmatrix}\Lambda_2\\1\end{bmatrix} \tag{12}$$

with $\Lambda_i=\frac{\beta^2\alpha}{-\omega_i{}^2+\beta^2}$. We emphasize that in our subsequent nonlinear analysis, we require the left eigen-

vectors corresponding to eigenvalues $\lambda = i\omega_1$ and $\lambda = i\omega_2$ and these are

$$\mathbf{l_1} = \begin{bmatrix} \mathrm{L}_1 \; 1 \end{bmatrix}, \quad \mathbf{l_2} = \begin{bmatrix} \mathrm{L}_2 \; 1 \end{bmatrix}, \tag{13}$$

with $L_i = \dfrac{k_r\,\alpha}{-{\omega_i}^2 + \beta^2}$. These left eigenvectors play a vital role in the elimination of secular terms to obtain a convergence slow-flow equations in MMS. The nonlinear analysis of the system using MMS is presented next.

4.2 Nonlinear analysis using method of multiple scales

In this section, we use MMS to determine the approximate solution of Eq. (7) and later investigate the stability of different steady states. We first start with defining multiple time scales as

$$T_0 = t\,, \quad T_1 = \epsilon t\,, \tag{14}$$

with T_0 and T_1 as the fast and slow time scales, respectively. With the introduction of these time scales, the derivative operators get perturbed and can be expressed in new time scales as

$$\frac{\mathrm{d}}{\mathrm{d}t} = D_0 + \epsilon D_1\,, \quad \frac{\mathrm{d}^2}{\mathrm{d}t^2} = D_{0,0} + 2\epsilon D_{0,1}\,, \tag{15}$$

where $D_n = \dfrac{\partial}{\partial T_n}$ and $D_{m,n} = \dfrac{\partial^2}{\partial T_m \partial T_n}$. Following this, the solution of perturbed nonlinear equation (Eq. (7)) can be expressed as a series in powers of ϵ till $\mathcal{O}(\epsilon)$ as

$$\mathbf{y}(\tau) = \mathbf{y_0}\,(T_0, T_1) + \epsilon \mathbf{y_1}\,(T_0, T_1) = \mathbf{y_0} + \epsilon \mathbf{y_1}\,, \tag{16}$$

with $\mathbf{y}(\tau) = [\eta(t),\ \vartheta(t)]^T$, $\mathbf{y}_m = \mathbf{y}_m(T_0,\ T_1)$. Having defined the approximate solution, next we first present the case of primary resonance.

4.3 Primary resonance near ω_1

To analyze primary resonances, we rescale the forcing term such that it appears in the same perturbation equation as the nonlinear terms and damping. Thus, we let $\bar{f_0} = \epsilon^2 f_0$ with $\omega_r = \omega_1 + \epsilon\sigma_1$ in Eq. (7) (where σ_1 is an external detuning parameter in the forcing frequency) in the perturbed nonlinear equations. On substituting Eqs. (15)–(16) in Eq. (7) and collecting different orders of ϵ, we get

$$\mathcal{O}(\epsilon^0) \quad : D_{0,0}\eta_0 + \beta^2\,(\eta_0 - \alpha\,\vartheta_0) = 0\,, \tag{17a}$$

$$D_{0,0}\vartheta_0 + \vartheta_0 - k_r\,\alpha\,(\eta_0 - \alpha\vartheta_0) = 0. \tag{17b}$$

$$\begin{aligned}\mathcal{O}(\epsilon) \quad & : D_{0,0}\eta_1 + \beta^2(\eta_1 - \alpha\vartheta_1) \\ & = -2\zeta\beta\,(D_0\eta_0 - \alpha D_0\vartheta_0) \\ & \quad - \alpha_1 m_r\,(\eta_0 - \alpha\vartheta_0)^2 - 2D_{0,1}\eta_0 \\ & \quad + f_0 m_r \cos(\omega_1 T_0 + \sigma_1 T_1),\end{aligned} \tag{18a}$$

$$\begin{aligned}& D_{0,0}\vartheta_1 + \vartheta_1 - k_r\alpha\,(\eta_1 - \alpha\vartheta_1) \\ & = 2\zeta\sqrt{\frac{k_r}{m_r}}\alpha\,(D_0\eta_0 - \alpha D_0\vartheta_0) - 2D_{0,1}\vartheta_0 \\ & \quad + \alpha_1\alpha(\eta_0 - \alpha\vartheta_0)^2 - q_{zr}\vartheta_0^2 \\ & \quad - 2\kappa D_0\vartheta_0 - f_0\alpha\cos\,(\omega_1\,T_0 + \sigma_1 T_1)\,.\end{aligned} \tag{18b}$$

Note that equations at $\mathcal{O}(\epsilon^0)$ for primary resonance are identical to the linearized unperturbed Eq. (8). Therefore, the solution of Eq. (17) can be written in vector form as

$$\begin{aligned}\mathbf{y}_0(T_0, T_1) = {} & A_1(T_1)\mathbf{r_1}e^{i\omega_1 T_1} \\ & + A_2(T_1)\mathbf{r_2}e^{i\omega_2 T_1} + \mathbf{C.C.}\,,\end{aligned} \tag{19}$$

where unlike the previous case A_1 and A_2 instead of being constants are the complex-valued functions of slow time T_1. On substituting the assumed solution for $\mathbf{y_0}$ in equations at $\mathcal{O}(\epsilon)$, i.e., Eq. (18) leads to the appearance of resonant forcing terms $e^{i\omega_1 T_0}, e^{i\omega_2 T_0}$, and consequentially their complex conjugate (the resulting equations are reported in Appendix-A). These resonant forcing terms cause the unbounded growth in the solution for $\mathbf{y}_1$ and are known as secular terms. Therefore, to obtain bounded solutions, it is required to eliminate these secular terms from the equations. The removal of secular terms from coupled ODEs further requires the dot product of the coefficient vectors corresponding to $\mathrm{e}^{i\omega_1 T_0}$ and $\mathrm{e}^{i\omega_2 T_0}$ with respect to left eigenvectors to be zero [44]. Furthermore, for the current analysis we can have two cases, (1) $1:2$ internal resonance, i.e., $\omega_1 \approx 2\omega_2$ and (2) nonresonance case (ω_1 is far away from ω_2). However, it is a well-established fact that, for the latter case, nonlinear terms do not contribute in any secular terms and hence do not affect the solution till the first order of approximation [37,43]. Hence, for the sake of brevity, we only present the first case, i.e., $1:2$ internal resonance. In this case, the natural frequencies of the system are nearly commensurate and accordingly, we can introduce an internal detuning parameter, σ_2, in the system as $\omega_1 = 2\omega_2 - \epsilon\sigma_2$, which

further leads to the following transformations

$$(\omega_1 - \omega_2)T_0 = (\omega_2 - \epsilon\sigma_2)T_0 = \omega_2 T_0 - \sigma_2 T_1,$$
$$2\omega_2 T_0 = (\omega_1 + \epsilon\sigma_2)T_0 = \omega_1 T_0 + \sigma_2 T_1 .$$

On substituting the above transformations in resulting equations (Appendix-A) and using the solvability condition of $\mathbf{l_1} \cdot \mathbf{u_1} = 0$ and $\mathbf{l_2} \cdot \mathbf{u_2} = 0$, where $\mathbf{u_1}$ and $\mathbf{u_2}$ are the coefficient vectors for $e^{i\omega_1 T_0}$ and $e^{i\omega_2 T_0}$, we get

$$R_{n2} = -l_n R_{n1}, \tag{20}$$

where

$$\begin{aligned}
R_{11} &= 2i\omega_1 \Lambda_1 D_1 A_1 + \mathrm{e}^{i\sigma_2 T_1} {A_2}^2 \alpha_1 m_r \ (\alpha - \Lambda_2)^2 \\
&\quad - \frac{f_0}{2} m_r \mathrm{e}^{i\sigma_1 T_1} - 2\,i A_1 \zeta \ (\alpha - \Lambda_1)\,\beta\,\omega_1 , \\
R_{12} &= 2i\omega_1 D_1 A_1 - {A_2}^2 \alpha_1 \alpha \ (\alpha - \Lambda_2)^2 \,\mathrm{e}^{i\sigma_2 T_1} \\
&\quad + \frac{f_0}{2} \alpha \mathrm{e}^{i\sigma_1 T_1} + q_{zr} {A_2}^2 \mathrm{e}^{i\sigma_2 T_1} \\
&\quad + 2\,i A_1 \sqrt{\frac{k_r}{m_r}} \zeta \ (\alpha - \Lambda_1)\,\omega_1 + 2i\kappa A_1 \omega_1, \\
R_{21} &= 2i\omega_2 \Lambda_2 D_1 A_2 + 2A_1 \bar{A}_2 \alpha_1 m_r \\
&\quad (\alpha - \Lambda_1)\left(\alpha - \bar{\Lambda}_2\right) \mathrm{e}^{-i\sigma_2 T_1} \\
&\quad - 2i A_2 \zeta \beta \omega_2 \ (\alpha - \Lambda_2) \ , \\
R_{22} &= 2i\omega_2 D_1 A_2 - 2A_1 \bar{A}_2 \alpha_1 \alpha \\
&\quad (\alpha - \Lambda_1)\left(\alpha - \bar{\Lambda}_2\right) \mathrm{e}^{-i\sigma_2 T_1} \\
&\quad + 2\mathrm{e}^{-i\sigma_2 T_1} q_{zr} A_1 \bar{A}_2 \\
&\quad + 2i A_2 \sqrt{\frac{k_r}{m_r}} \zeta \alpha \omega_2 \ (\alpha - \Lambda_2) + 2i\kappa\omega_2 A_2 .
\end{aligned}$$

As it is convenient to express A_n and $\bar{A}_n$ (for $n = 1,\ 2$) in polar notation for further analysis, we put

$$A_n = \frac{a_n(T_1)}{2}\mathrm{e}^{i\beta(T_1)} \quad \bar{A}_n = \frac{a_n(T_1)}{2}\mathrm{e}^{-i\beta(T_1)} \quad \text{for } n = 1,\ 2 \tag{21}$$

and consequently their complex conjugate in Eq. (20). Note that a_n and β_n (for $n = 1, 2$) are real function of T_1 instead of being constants unlike the nonresonant case [43].

Substituting this transformation in Eq. (20) and solving for $D_1 a_n$ and $D_1 \beta_n$ (for $n = 1, 2$), we get the slow-flow equations as

$$D_1 a_1 = \Gamma_1 a_1 + \Gamma_2 \sin(\gamma_1) a_2^2 + f_0 \Gamma_3 \sin(\gamma_2) , \tag{22a}$$
$$\begin{aligned}
D_1 \gamma_1 &= \sigma_2 + 2D_1\beta_2 - D_1\beta_1 = \sigma_2 + 2\Gamma_4 a_1 \cos(\gamma_1) \\
&\quad + \Gamma_2 \cos(\gamma_1)\frac{a_2^2}{a_1} \\
&\quad + f_0 \Gamma_3 \cos(\gamma_2)\frac{1}{a_1} ,
\end{aligned} \tag{22b}$$
$$D_1 a_2 = \Gamma_4 \sin(\gamma_1) a_2 a_1 + \Gamma_5 a_2 , \tag{22c}$$
$$\begin{aligned}
D_1 \gamma_2 &= \sigma_1 - D_1\beta_1 = \sigma_1 + \Gamma_2 \cos(\gamma_1)\frac{a_2^2}{a_1} \\
&\quad + f_0 \Gamma_3 \cos(\gamma_2)\frac{1}{a_1} ,
\end{aligned} \tag{22d}$$

where Γ_n (for n=1,2,..5) are defined in Appendix-A. For the steady-state response $D_1 a_n = D_1 \gamma_n = 0$, which further leads to

$$\sin(\gamma_1^*) = -\frac{\Gamma_5}{\Gamma_4 a_1^*}, \quad \cos(\gamma_1^*) = -\frac{\sigma_2 - \sigma_1}{2\Gamma_4 a_1^*} . \tag{23a}$$
$$\begin{aligned}
\sin(\gamma_2^*) &= -\frac{\Gamma_4 {a_1^*}^2 \Gamma_1 - \Gamma_2 {a_2^*}^2 \Gamma_5}{\Gamma_4 a_1^* f_0 \Gamma_3}, \\
\cos(\gamma_2^*) &= -\frac{2\,\Gamma_4 \sigma_1 {a_1^*}^2 - \sigma_2 {a_2^*}^2 \Gamma_2 + \sigma_1 {a_2^*}^2 \Gamma_2}{2\Gamma_4 a_1^* f_0 \Gamma_3} .
\end{aligned} \tag{23b}$$

In the above and subsequent expressions for steady states, superscript $(*)$ corresponds to steady-state quantities. Next, by using trigonometric identity, the above expressions can be solved for the steady states, a_1^* and a_2^*, to obtain

$$a_1^* = \frac{\sqrt{4\,{\Gamma_5}^2 + {\sigma_1}^2 - 2\,\sigma_1\,\sigma_2 + {\sigma_2}^2}}{2\Gamma_4} , \tag{24a}$$
$$a_2^* = \sqrt{\frac{\sigma_1\,\sigma_2 + 2\,\Gamma_5\,\Gamma_1 - {\sigma_1}^2 \pm \sqrt{4\,{\Gamma_4}^2 {f_0}^2 {\Gamma_3}^2 - (\Gamma_1\,\sigma_2 - 2\,\Gamma_5\,\sigma_1 - \Gamma_1\,\sigma_1)^2}}{2\Gamma_2\Gamma_4}} . \tag{24b}$$

However, from Eq. (22c) we observe that $a_2 = 0$ is also a solution which further leads to another set of steady states as

$$a_1^* = \pm\frac{f_0\Gamma_3}{\sqrt{\sigma_1^2+\Gamma_1^2}},\ a_2^* = 0,\ \sin(\gamma_2^*) = -\frac{\Gamma_1 a_1^*}{f_0\Gamma_3},\ \cos(\gamma_2^*) = -\frac{\sigma_1 a_1^*}{f_0\Gamma_3}. \tag{25}$$

Note that there is no effect of nonlinearity on steady states for the latter set of steady states (Eq. (25)). Therefore, it essentially forms a solution of the linear problem unlike the previous set (Eq (24)) of steady states. Furthermore, we observe that for steady states given by Eq. (24), the mode corresponding to ω_1 is independent of excitation amplitude, f_0, although the excitation frequency is close to ω_1, while the other mode a_2 is getting excited directly from f_0. Having obtained the steady states, the first-order solution of the system can be written using Eqs. (16)–(19)–(21)–(19)–(23)–(24) and is

$$\eta(t) = \Lambda_1 a_1^*\cos(\omega_r t-\gamma_2) + \Lambda_2 a_2^*\cos\left(\frac{1}{2}(\omega_r t+\gamma_1-\gamma_2)\right)+\mathcal{O}(\epsilon), \tag{26a}$$

$$\vartheta(t) = a_1^*\cos(\omega_r t-\gamma_2) + a_2^*\cos\left(\frac{1}{2}(\omega_r t+\gamma_1-\gamma_2)\right)+\mathcal{O}(\epsilon). \tag{26b}$$

Next we present the case of primary resonance near lower natural frequency, i.e., ω_2.

4.4 Primary resonance near ω_2

In this case, we let $\omega_r = \omega_2 + \epsilon\sigma_1$ along with $\bar{f}_0 = \epsilon^2 f_0$, Eqs. (15)–(16) in Eq. (7) and collect different orders of ϵ to get equations governing the evolution of η_n, and ϑ_n (reported in Appendix-B). Following the procedure as in the case of primary resonance near ω_1, we get the slow-flow equations as

$$D_1 a_1 = \Gamma_1 a_1 + \Gamma_2\sin(\gamma_1)a_2^2, \tag{27a}$$

$$D_1\gamma_1 = \sigma_2 + 2D_1\beta_2 - D_1\beta_1 = \sigma_2 - 2f_0\Gamma_3\cos(\gamma_2)\frac{1}{a_2} + 2\Gamma_4 a_1\cos(\gamma_1) + \Gamma_2\cos(\gamma_1)\frac{a_2^2}{a_1}, \tag{27b}$$

$$D_1 a_2 = f_0\Gamma_3\sin(\gamma_2) + \Gamma_4\sin(\gamma_1)a_2 a_1 + \Gamma_5 a_2, \tag{27c}$$

$$D_1\gamma_2 = \sigma_1 - D_1\beta_2 = \sigma_1 - \Gamma_4\cos(\gamma_1)a_1 + f_0\Gamma_3\cos(\gamma_2)\frac{1}{a_2}, \tag{27d}$$

where Γ_n (for $n = 1, 2, \cdots, 5$) are defined in Eq. 23. For the steady-state response, we let $D_1 a_n = D_1\gamma_n = 0$ in Eq. (27) and accordingly get

$$\sin(\gamma_1^*) = -\frac{\Gamma_1 a_1^*}{\Gamma_2 a_2^{*2}},\qquad \cos(\gamma_1^*) = \frac{-\Gamma_2 a_2^{*2}\Gamma_5 + \Gamma_4 a_1^{*2}\Gamma_1}{\Gamma_2 a_2^*\Gamma_3 f_0}, \tag{28a}$$

$$\sin(\gamma_2^*) = -\frac{a_1^*(\sigma_2+2\sigma_1)}{\Gamma_2 a_2^{*2}},\qquad \cos(\gamma_2^*) = -\frac{\sigma_1 a_2^{*2}\Gamma_2 + \Gamma_4 a_1^{*2}\sigma_2 + 2\Gamma_4 a_1^{*2}\sigma_1}{\Gamma_2 a_2^*\Gamma_3 f_0}, \tag{28b}$$

which further leads us to the equations governing a_1^* and a_2^* as

$$a_1^* = \frac{\Gamma_2 a_2^{*2}}{\sqrt{{\Gamma_1}^2+{\sigma_2}^2+4\sigma_2\sigma_1+4{\sigma_1}^2}}, \tag{29a}$$

$$\begin{aligned}&{\Gamma_2}^4{\Gamma_4}^2{a_2}^6 + {\Gamma_2}^2(-2\Gamma_2\Gamma_5\Gamma_4\Gamma_1 + 2\sigma_1\Gamma_2\Gamma_4\sigma_2 + 4{\sigma_1}^2\Gamma_2\Gamma_4){a_2}^4 \\ &+{\Gamma_2}^2\left({\sigma_2}^2{\sigma_1}^2 + 4{\sigma_1}^4 + {\gamma_1}^2{\Gamma_5}^2 + 4{\Gamma_5}^2{\sigma_1}^2 + {\Gamma_1}^2{\sigma_1}^2 + 4\sigma_2{\sigma_1}^3 + 4{\Gamma_5}^2\sigma_2\sigma_1 + {\Gamma_5}^2{\sigma_2}^2\right){a_2}^2 \\ &+{\Gamma_2}^2\left(-4{\Gamma_3}^2{f_0}^2\sigma_2\sigma_1 - {\Gamma_1}^2{\Gamma_3}^2{f_0}^2 - {\Gamma_3}^2{f_0}^2{\sigma_2}^2 - 4{\Gamma_3}^2{f_0}^2{\sigma_1}^2\right) = 0\end{aligned} \tag{29b}$$

From Eq. (29), it can be observed that unlike the case of primary resonance near ω_1, both steady states of both modes, i.e., a_1^* and a_2^*, are excited by the external forcing. Using these steady-state quantities, the first-order solution of the system in this case can be written as

$$\eta(t) = \Lambda_1 a_1^*\cos(2\omega_r t-2\gamma_2-\gamma_1) + \Lambda_2 a_2^*\cos(\omega_r t-\gamma_2))+\mathcal{O}(\epsilon), \tag{30a}$$

$$\vartheta(t) = a_1^*\cos(2\omega_r t-2\gamma_2-\gamma_1) + a_2^*\cos(\omega_r t-\gamma_2)+\mathcal{O}(\epsilon). \tag{30b}$$

Having established the first-order solution for both cases of primary resonance, next, we present the case of secondary resonance.

4.5 Secondary resonance

For secondary resonance, the excitation frequency ω_r is not close to the natural frequencies ω_1 and ω_2, and the effect of external forcing will be not captured unless $\bar{f}_0$ is a $\mathcal{O}(1)$ quantity. Therefore, we substitute $\bar{f}_0 = \epsilon f_0$ along with Eqs. (15)–(16) in Eq. (7) and collect different orders of ϵ to get

$$\begin{aligned}\mathcal{O}(\epsilon^0) \quad &: D_{0,0}\eta_0 \\ &+ \beta^2 (\eta_0 - \alpha\, \vartheta_0) = f_0 m_r \cos(\omega_1 T_0)\,, \qquad (31a)\\ D_{0,0}\vartheta_0 &+ \vartheta_0 \\ &- k_r\, \alpha\, (\eta_0 - \alpha\vartheta_0) = -f_0 \alpha \cos(\omega_r\, T_0)\,. \qquad (31b)\end{aligned}$$

$$\begin{aligned}\mathcal{O}(\epsilon) \quad &: D_{0,0}\eta_1 + \beta^2(\eta_1 - \alpha\vartheta_1) \\ &= -2\zeta\beta\, (D_0\eta_0 - \alpha D_0\vartheta_0) \\ &\quad - \alpha_1 m_r\, (\eta_0 - \alpha\vartheta_0)^2 - 2D_{0,1}\eta_0, \qquad (32a)\\ D_{0,0}\vartheta_1 &+ \vartheta_1 - k_r\alpha\, (\eta_1 - \alpha\vartheta_1) \\ &= 2\zeta\sqrt{\frac{k_r}{m_r}}\alpha\, (D_0\eta_0 - \alpha D_0\vartheta_0) \\ &\quad - 2D_{0,1}\vartheta_0 + \alpha_1\alpha(\eta_0 - \alpha\vartheta_0)^2 \\ &\quad - q_{zr}\vartheta_0^2 - 2\kappa D_0\vartheta_0. \qquad (32b)\end{aligned}$$

The solution of Eq. (31) can be expressed in the form of

$$\begin{aligned}\mathbf{y}_0(T_0, T_1) = A_1(T_1)\mathbf{r_1}e^{i\omega_1 T_1} + A_2(T_1)\mathbf{r_2}e^{i\omega_2 T_1} \\ + f_0\boldsymbol{\Phi}\cos(\omega_r T_0) + \mathbf{C.C.}\,, \qquad (33)\end{aligned}$$

where $\boldsymbol{\Phi}$ is a vector with coefficients corresponding to the forced response of the system (obtained by the harmonic balance method) and is

$$\boldsymbol{\Phi} = \begin{bmatrix}\Phi_1 \\ \Phi_2\end{bmatrix} \qquad (34)$$

where

$$\begin{aligned}\Phi_1 &= \frac{\left(\beta^2\alpha^2 - m_r + {\omega_r}^2 m_r - k_r\,\alpha^2 m_r\right)}{(\omega_r^2 - 1)(\beta^2 - \omega_r^2) + k_r\alpha^2\omega_r^2} \quad \text{and} \\ \Phi_2 &= \frac{\alpha\left(\beta^2 - {\omega_r}^2 - k_r\, m_r\right)}{(\omega_r^2 - 1)(\beta^2 - \omega_r^2) + k_r\alpha^2\omega_r^2}\,. \qquad (35)\end{aligned}$$

The resulting equations, after the substitution of the assumed form of the solution, are reported in Appendix-C. In the resulting equations, CVF_1 and CVF_2 represent the complex-valued functions and do not contribute to secular terms. It can be observed from these equations that in addition to the terms proportional to $e^{i\omega_n T_0}$, secular terms can originate when $\omega_r = \omega_n/2$, $\omega_r = 2\omega_n$, and $\omega_r = \omega_1 \pm \omega_2$ due to the appearance of $e^{2i\omega_r T_0}$, $e^{i\omega_r \pm \omega_1}$ and $e^{i\omega_r \pm \omega_2}$. These cases of resonance are referred as secondary resonance. In this work, we are particularly considering two special cases (1) $2\omega_r \approx \omega_i$, and (2) $\omega_r \approx \omega_1 + \omega_2$ also referred as superharmonic resonance and combined resonance, respectively. We start with the case of superharmonic resonance near ω_1.

4.5.1 Superharmonic resonance near ω_1

For the superharmonic resonance near ω_1, we again introduce an external and internal detuning parameter, i.e., σ_1 and σ_2, in the system as $2\omega_2 = \omega_1 + \epsilon\sigma_2$. On substituting this transformation in the resulting equations (Appendix-C) and following the procedure for the removal of secular terms, we get the slow-flow equations as

$$\begin{aligned}D_1 a_1 &= \Gamma_1 a_1 + \Gamma_2 \sin(\gamma_1) a_2^2 + f_0^2\Gamma_3 \sin(\gamma_2), \qquad (36a)\\ D_1\gamma_1 &= \sigma_2 + 2D_1\beta_2 - D_1\beta_1 = \sigma_2 + 2\Gamma_4\cos(\gamma_1)a_1 \\ &\quad + \Gamma_2\cos(\gamma_1)\frac{a_2^2}{a_1} + f_0^2\frac{\Gamma_3\cos(\gamma_2)}{a_1}, \qquad (36b)\\ D_1 a_2 &= \Gamma_4\sin(\gamma_1)a_2 a_1 + \Gamma_5 a_2, \qquad (36c)\\ D_1\gamma_2 &= \sigma_1 - D_1\beta_1 = \sigma_1 \\ &\quad + \Gamma_2\cos(\gamma_1)\frac{a_2^2}{a_1} + f_0^2\frac{\Gamma_3\cos(\gamma_2)}{a_1}, \qquad (36d)\end{aligned}$$

where Γ_n (for n=1,2,..5) are defined in Appendix-D. The condition for steady-state response (i.e., $D_1 a_n = D_1\gamma_n = 0$) in Eq. (36) leads to

$$\begin{aligned}\sin(\gamma_1^*) &= -\frac{\Gamma_5}{\Gamma_4\, a_1^*}, \quad \cos(\gamma_1^*) = -\frac{\sigma_2 - \sigma_1}{2\Gamma_4\, a_1^*} \qquad (37a)\\ \sin(\gamma_2^*) &= -\frac{\Gamma_4\, {a_1^*}^2\Gamma_1 - \Gamma_2\, {a_2^*}^2\Gamma_5}{\Gamma_4\, a_1^*\, f_0^2\, \Gamma_3}, \\ \cos(\gamma_2^*) &= -\frac{2\,\Gamma_4\,\sigma_1\, {a_1^*}^2 - \sigma_2 {a_2^*}^2\Gamma_2 + \sigma_1\, {a_2^*}^2\Gamma_2}{2\Gamma_4\, a_1^*\, f_0^2\, \Gamma_3}\,. \qquad (37b)\end{aligned}$$

Using the above expressions and trigonometric identity, we further obtain a_1^* and a_2^* as

$$a_1^* = \frac{\sqrt{4\,\Gamma_5{}^2 + \sigma_1{}^2 - 2\,\sigma_1\,\sigma_2 + \sigma_2{}^2}}{2\Gamma_4}\,, \tag{38a}$$

$$a_2^* = \sqrt{\frac{\sigma_1\,\sigma_2 + 2\,\Gamma_5\,\Gamma_1 - \sigma_1{}^2 \pm \sqrt{4\,\Gamma_4{}^2 f_0{}^4 \Gamma_3{}^2 - (\Gamma_1\,\sigma_2 - 2\,\Gamma_5\,\sigma_1 - \Gamma_1\,\sigma_1)^2}}{2\Gamma_2\Gamma_4}}\,. \tag{38b}$$

Again, another set of steady-state solution exists for the system similar to the primary resonance case near ω_1 and is

$$a_1^* = \pm\frac{f_0^2\Gamma_3}{\sqrt{\sigma_1^2 + \Gamma_1^2}},\ a_2^* = 0,\ \sin(\gamma_1^*) = -\frac{\Gamma_1 a_1^*}{f_0^2\Gamma_3},$$
$$\cos(\gamma_2^*) = -\frac{\sigma_1 a_1^*}{f_0^2\Gamma_3}\,. \tag{39}$$

Using these steady-state quantities, the first-order approximate solution of the system can be obtained as

$$\begin{aligned}\eta(t) &= \Lambda_1 a_1^*\cos(2\omega_r t - \gamma_2)\\ &\quad + \Lambda_2 a_2^*\cos\left(\frac{1}{2}(2\omega_r t + \gamma_1 - \gamma_2)\right)\\ &\quad + f_0\Phi_1\cos(\omega_r t) + \mathcal{O}(\epsilon)\,,\end{aligned} \tag{40a}$$

$$\begin{aligned}\vartheta(t) &= a_1^*\cos(2\omega_r t - \gamma_2) + a_2^*\\ &\quad \times\cos\left(\frac{1}{2}(2\omega_r t + \gamma_1 - \gamma_2)\right)\\ &\quad + f_0\Phi_2\cos(\omega_r t) + \mathcal{O}(\epsilon)\,.\end{aligned} \tag{40b}$$

After getting the first-order solution for the case of superharmonic resonance near ω_1, next we present the case of superharmonic resonance near ω_2.

4.5.2 Superharmonic resonance near ω_2

Similar to the case of superharmonic resonance near ω_1, for the case of superharmonic resonance near ω_2, we introduce an external and internal detuning parameter in the system as

$$2\omega_r = \omega_2 + \epsilon\sigma_1 \quad \text{and} \quad 2\omega_2 = \omega_1 + \epsilon\sigma_2. \tag{41}$$

Again, substituting back these transformations in the resulting equations (Appendix-C) and removing secular terms from equations lead to slow-flow equations as

$$D_1 a_1 = \Gamma_1 a_1 + \Gamma_2\sin(\gamma_1)a_2^2 \tag{42a}$$

$$D_1\gamma_1 = \sigma_2 + 2D_1\beta_2 - D_1\beta_1 = \sigma_2 - f_0^2\frac{2\Gamma_3\cos(\gamma_2)}{a_2} + 2\Gamma_4\cos(\gamma_1)a_1 + \Gamma_2\cos(\gamma_1)\frac{a_2^2}{a_1} \tag{42b}$$

$$D_1 a_2 = \Gamma_3 f_0^2\sin(\gamma_2) + \Gamma_4\sin(\gamma_1)a_1 a_2 + \Gamma_5 a_2 \tag{42c}$$

$$D_1\gamma_2 = \sigma_1 - D_1\beta_2 = \sigma_1 + f_0^2\frac{\Gamma_3\cos(\gamma_2)}{a_2} - \Gamma_4\cos(\gamma_1)a_1 \tag{42d}$$

where Γ_n (for $n = 1, 2, \cdots, 5$) are defined in Appendix-D. For the steady-state response, i.e., $D_1 a_n = D_1\gamma_n = 0$, Eq. (42) can be solved for steady states as

$$\sin(\gamma_1^*) = -\frac{\Gamma_1\,a_1^*}{\Gamma_2\,a_2^{*2}},$$
$$\cos(\gamma_1^*) = -\frac{a_1^*\,(\sigma_2 + 2\,\sigma_1)}{\Gamma_2\,a_2^{*2}} \tag{43a}$$

$$\sin(\gamma_2^*) = \frac{-\Gamma_2\,a_2^{*2}\Gamma_5 + \Gamma_4\,a_1^{*2}\Gamma_1}{\Gamma_2\,a_2^*\,\Gamma_3\,f_0^2},$$
$$\cos(\gamma_2^*) = -\frac{\sigma_1\,a_2^{*2}\Gamma_2 + \Gamma_4\,a_1^{*2}\sigma_2 + 2\,\Gamma_4\,a_1^{*2}\sigma_1}{\Gamma_2\,a_2^*\,\Gamma_3\,f_0^2}\,. \tag{43b}$$

Again, by using trigonometric identity we get the equations governing a_1^* and a_2^* as

$$a_1^* = \frac{\Gamma_2\,a_2^{*2}}{\sqrt{\Gamma_1{}^2 + \sigma_2{}^2 + 4\,\sigma_2\,\sigma_1 + 4\,\sigma_1{}^2}}, \tag{44a}$$

$$\begin{aligned}&\Gamma_2{}^4\Gamma_4{}^2 a_2{}^6 + \Gamma_2{}^2\Big(-2\,\Gamma_2\,\Gamma_5\,\Gamma_4\,\Gamma_1 + 2\,\sigma_1\,\Gamma_2\,\Gamma_4\\ &\quad \sigma_2 + 4\,\sigma_1{}^2\Gamma_2\,\Gamma_4\Big)\,a_2{}^4\\ &\quad +\Gamma_2{}^2\Big(\sigma_2{}^2\sigma_1{}^2 + 4\,\sigma_1{}^4 + \gamma_1{}^2\Gamma_5{}^2\\ &\quad +4\,\Gamma_5{}^2\sigma_1{}^2 + \Gamma_1{}^2\sigma_1{}^2\\ &\quad +4\,\sigma_2\,\sigma_1{}^3 + 4\,\Gamma_5{}^2\sigma_2\,\sigma_1 + \Gamma_5{}^2\sigma_2{}^2\Big)\,a_2{}^2\\ &\quad +\Gamma_2{}^2\Big(-4\,\Gamma_3{}^2 f_0{}^4\sigma_2\,\sigma_1 - \Gamma_1{}^2\Gamma_3{}^2 f_0{}^4\\ &\quad -\Gamma_3{}^2 f_0{}^4\sigma_2{}^2 - 4\,\Gamma_3{}^2 f_0{}^4\sigma_1{}^2\Big) = 0\end{aligned} \tag{44b}$$

From Eq. (44), it can be observed that unlike the previous case of superharmonic resonance, both modes, i.e., a_1 and a_2, are excited by the external forcing. Using these steady-state quantities, the first-order solution of the system in this case will be

$$\begin{aligned}\eta(t) &= \Lambda_1 a_1^* \cos(4\omega_r t - 2\gamma_2 - \gamma_1) \\ &\quad + \Lambda_2 a_2^* \cos(2\omega_r t - \gamma_2)) \\ &\quad + f_0 \Phi_1 \cos(\omega_r t)\mathcal{O}(\epsilon) \qquad (45a)\\ \vartheta(t) &= a_1^* \cos(4\omega_r t - 2\gamma_2 - \gamma_1) \\ &\quad + a_2^* \cos(2\omega_r t - \gamma_2) \\ &\quad + f_0 \Phi_2 \cos(\omega_r t) + \mathcal{O}(\epsilon) \qquad (45b)\end{aligned}$$

Having established the first-order solution for superharmonic resonance near ω_2, next we present the case of combined resonance.

4.5.3 Combined resonance

For the case of combined resonance, the excitation frequency is close to the sum of the natural frequencies of the system, i.e., $\omega_r \approx \omega_1 + \omega_2$, and accordingly, we introduce an external detuning parameter in the system as

$$\omega_r = \omega_1 + \omega_2 + \epsilon\sigma_1 \,. \qquad (46)$$

Substitution of the above transformation along with the internal detuning parameter for the case of internal resonance in the resulting equations in Appendix-D and removal of secular terms leads to the slow-flow equations as

$$\begin{aligned}D_1 a_1 &= \Gamma_1 a_1 + \Gamma_2 \sin(\gamma_1) a_2^2 + \Gamma_3 \sin(\gamma_2) f_0 a_2 \,, \qquad (47a)\\ D_1\gamma_1 &= \sigma_2 + 2D_1\beta_2 - D_1\beta_1 \\ &= \sigma_2 + 2\,\Gamma_4 \cos(\gamma_1)\, a_1 \\ &\quad - 2\,\frac{f_0\,\Gamma_5 \cos(\gamma_2)\, a_1}{a_2} + \frac{\Gamma_2 \cos(\gamma_1)\, {a_2}^2}{a_1} \\ &\quad + \frac{\Gamma_3 \cos(\gamma_2)\, f_0\, a_2}{a_1} \,, \qquad (47b)\\ D_1 a_2 &= \Gamma_4 \sin(\gamma_1) a_2 a_1 + f_0 \Gamma_5 \sin(\gamma_2) \\ &\quad + \Gamma_4 \sin(\gamma_1) a_1 a_2 + \Gamma_5 a_2 \,, \qquad (47c)\\ D_1\gamma_2 &= \sigma_1 - D_1\beta_1 - D_1\beta_2 = \sigma_1 + \frac{\Gamma_2 \cos(\gamma_1)\, {a_2}^2}{a_1} \\ &\quad + \frac{\Gamma_3 \cos(\gamma_2)\, f_0\, a_2}{a_1} - \Gamma_4 \cos(\gamma_1)\, a_1 \\ &\quad + \frac{f_0 \Gamma_5 \cos(\gamma_2) a_1}{a_2} \qquad (47d)\end{aligned}$$

where Γ_n (for $n = 1, 2, \ldots, 5$) are defined in Appendix-E. Again, for the steady-state condition, i.e., $D_1 a_n = D_1\gamma_n = 0$, in Eq. (47) leads to

$$\begin{aligned}\sin(\gamma_1^*) &= -\frac{\Gamma_1 {a_1^*}^2 \Gamma_5 - \Gamma_3 {a_2^*}^2 \Gamma_6}{a_1^*\,(\Gamma_2\,\Gamma_5 - \Gamma_4\,\Gamma_3)\,{a_2^*}^2}, \\ \cos(\gamma_1^*) &= -\frac{2\,{a_1^*}^2\Gamma_5\,\sigma_1 + {a_1^*}^2\Gamma_5\,\sigma_2 - \Gamma_3\,{a_2^*}^2\sigma_1 + \Gamma_3\,{a_2^*}^2\sigma_2}{3\,(\Gamma_4\,\Gamma_3 + \Gamma_2\,\Gamma_5)\,a_1^*\,{a_2^*}^2} \qquad (48a)\\ \sin(\gamma_2^*) &= \frac{-\Gamma_2\,{a_2^*}^2\Gamma_6 + \Gamma_4\,{a_1^*}^2\Gamma_1}{a_2^*\,f_0\,a_1^*\,(\Gamma_2\,\Gamma_5 - \Gamma_4\,\Gamma_3)}, \\ \cos(\gamma_2^*) &= -\frac{2\,{a_1^*}^2\Gamma_4\,\sigma_1 + {a_1^*}^2\Gamma_4\,\sigma_2 - {a_2^*}^2\Gamma_2\,\sigma_2 + {a_2^*}^2\Gamma_2\,\sigma_1}{3a_2^*\,f_0\,a_1^*\,(\Gamma_4\,\Gamma_3 + \Gamma_2\,\Gamma_5)} \qquad (48b)\end{aligned}$$

From the above expressions, we can get the equations governing a_1^* and a_2^* as

$$\begin{aligned}&\left(\frac{\Gamma_1\,{a_1^*}^2\Gamma_5 - \Gamma_3\,{a_2^*}^2\Gamma_6}{a_1^*\,(\Gamma_2\,\Gamma_5 - \Gamma_4\,\Gamma_3)\,{a_2^*}^2}\right)^2 \\ &\quad + \left(\frac{2\,{a_1^*}^2\Gamma_5\,\sigma_1 + {a_1^*}^2\Gamma_5\,\sigma_2 - \Gamma_3\,{a_2^*}^2\sigma_1 + \Gamma_3\,{a_2^*}^2\sigma_2}{3\,(\Gamma_4\,\Gamma_3 + \Gamma_2\,\Gamma_5)\,a_1^*\,{a_2^*}^2}\right)^2 = 1 \qquad (49a)\\ &\left(\frac{-\Gamma_2\,{a_2^*}^2\Gamma_6 + \Gamma_4\,{a_1^*}^2\Gamma_1}{a_2^*\,f_0\,a_1^*\,(\Gamma_2\,\Gamma_5 - \Gamma_4\,\Gamma_3)}\right)^2 \\ &\quad + \left(\frac{2\,{a_1^*}^2\Gamma_4\,\sigma_1 + {a_1^*}^2\Gamma_4\,\sigma_2 - {a_2^*}^2\Gamma_2\,\sigma_2 + {a_2^*}^2\Gamma_2\,\sigma_1}{3a_2^*\,f_0\,a_1^*\,(\Gamma_4\,\Gamma_3 + \Gamma_2\,\Gamma_5)}\right)^2 = 1 \qquad (49b)\end{aligned}$$

From Eq. (49), we get the steady states a_1^* and a_2^* and accordingly, the first-order solution of the system for the case of combined resonance will be

$$\begin{aligned}\eta(t) &= \Lambda_1 a_1^* \cos\left(\frac{2}{3}\omega_r t - \frac{1}{3}\gamma_1 - \frac{2}{3}\gamma_2\right) \\ &\quad + \Lambda_2 a_2^* \cos\left(\frac{1}{3}\omega_r t + \frac{1}{3}\gamma_1 - \frac{1}{3}\gamma_2\right) \\ &\quad + f_0 \Phi_1 \cos(\omega_r t) + \mathcal{O}(\epsilon) \qquad (50a)\\ \vartheta(t) &= a_1^* \cos\left(\frac{2}{3}\omega_r t - \frac{1}{3}\gamma_1 - \frac{2}{3}\gamma_2\right) \\ &\quad \cos\left(\frac{1}{3}\omega_r t + \frac{1}{3}\gamma_1 - \frac{1}{3}\gamma_2\right) \\ &\quad + f_0 \Phi_2 \cos(\omega_r t) + \mathcal{O}(\epsilon) \qquad (50b)\end{aligned}$$

Having established the first-order solution for primary and secondary resonance, now we present the linear stability analysis of the steady states.

4.6 Linear stability of steady states

To determine stability of different steady states, we perturb the amplitude and phase from the steady-state values and substitute

$$a_1(T_1) = a_1^* + \epsilon a1(T_1), \tag{51}$$
$$a_2(T_1) = a_2^* + \epsilon a2(T_1), \tag{52}$$
$$\gamma_1(T_1) = \gamma_1^* + \epsilon \gamma 1(T_1), \tag{53}$$
$$\gamma_2(T_1) = \gamma_2^* + \epsilon \gamma 2(T_1), \tag{54}$$

in the slow-flow equations corresponding to primary and secondary resonances. On neglecting the higher order of ϵ, we get the set of four linear equations for each case of resonance, which can be further written in a compact form as

$$\dot{\mathbf{x}} = \mathbf{J}\mathbf{x} \tag{55}$$

where $\dot{\mathbf{x}}$ is $[a1,\ a2,\ \gamma 1,\ \gamma 2]^T$ and $\mathbf{J}$ is the Jacobian matrix. The Jacobian matrices for the case of the primary and secondary resonance, i.e., $\mathbf{J}_{P1}$, $\mathbf{J}_{S1}$, $\mathbf{J}_{P2}$, $\mathbf{J}_{S2}$, and $\mathbf{J}_C$, are defined in Appendix-F. Note that in the these matrices, subscript Pi and Si represent primary and superharmonic resonance near frequency ω_i, respectively, subscript C corresponds to combined resonance, and (*) represent the quantities corresponding to steady states. The eigenvalues of $\mathbf{J}_{Pi}$, $\mathbf{J}_{Si}$, and $\mathbf{J}_C$ govern the stability of steady states for primary , superharmonic, and combined resonance, respectively. If all four eigenvalues have negative real part, then the steady states are considered to be stable, otherwise unstable. Next, we present a detailed analysis of these steady states with numerical validation.

5 Result and discussion

In this section, a detailed analysis of the forced vibrations of the UPM machine with nonlinear isolators is presented. We have used the parameter values listed in Table 1 for numerical and analytical simulations.

The first part of the analysis is to validate the derived analytical closed-form expressions and determine the value of ϵ (depends on the system parameters) that validates our assumption of a weakly nonlinear system. For this purpose, we compare the analytical solutions, obtained using MMS, with numerical solution of the system given by Eq. (5). The initial condition for the numerical simulation is chosen corresponding to steady states.

Table 1 Nondimensional parameters of UPM machine used in the analysis

Parameter	Value
ζ	0.001
κ	0.001
β	0.83
α_1	0.0246
m_r	0.9333
q_{zr}	0.0983
k_r	0.7333

For the numerical simulations, we have used MATLAB routine 'ode45' with high relative and absolute tolerance ($1e^{-10}$). The comparisons between the numerical simulation of the system given by Eq. (5) and the analytical results from MMS for primary resonance near ω_1 (Eq. (25)) are shown in Fig. 4, with $1:2$ complete internal resonance, i.e., $\sigma_2 = 0$. From Fig. 4, we can observe that there is an excellent agreement between the numerical simulations and analytical solutions for the value of $\epsilon = 0.0001$. This agreement between the analytical and numerical simulation can be further observed for the other cases of resonances considered in this work (shown in Figs. 5, 6, 7 and 8) for $\epsilon = 0.0001$. To further verify the analytical solutions obtained using MMS, we compare the analytical force response curve of the system with that obtained numerically. For this, we solve the governing equations of motion for different cases of resonance using MATLAB routine 'ode45' with high values of relative and absolute tolerance ($1e^{-10}$) and decreasing values of f_0. Figures 9, 10, and 11 show the extrema of $y(\tau)$, obtained numerically and analytically, for the steady- state response with $\epsilon = 0.0001$. From these figures, we can observe an excellent match between both approaches for the given value of ϵ. This observation further validates our analytical approach. Therefore, in the remaining analysis we have chosen the value of $\epsilon = 0.0001$.

Having established the agreement between the analytical and numerical simulations, now we present the force and frequency responses of the system for the different cases of resonances. At first, we present the resonance cases when the primary and secondary resonances (superharmonic resonance) are close to the higher natural frequency of the system, i.e., ω_1. The

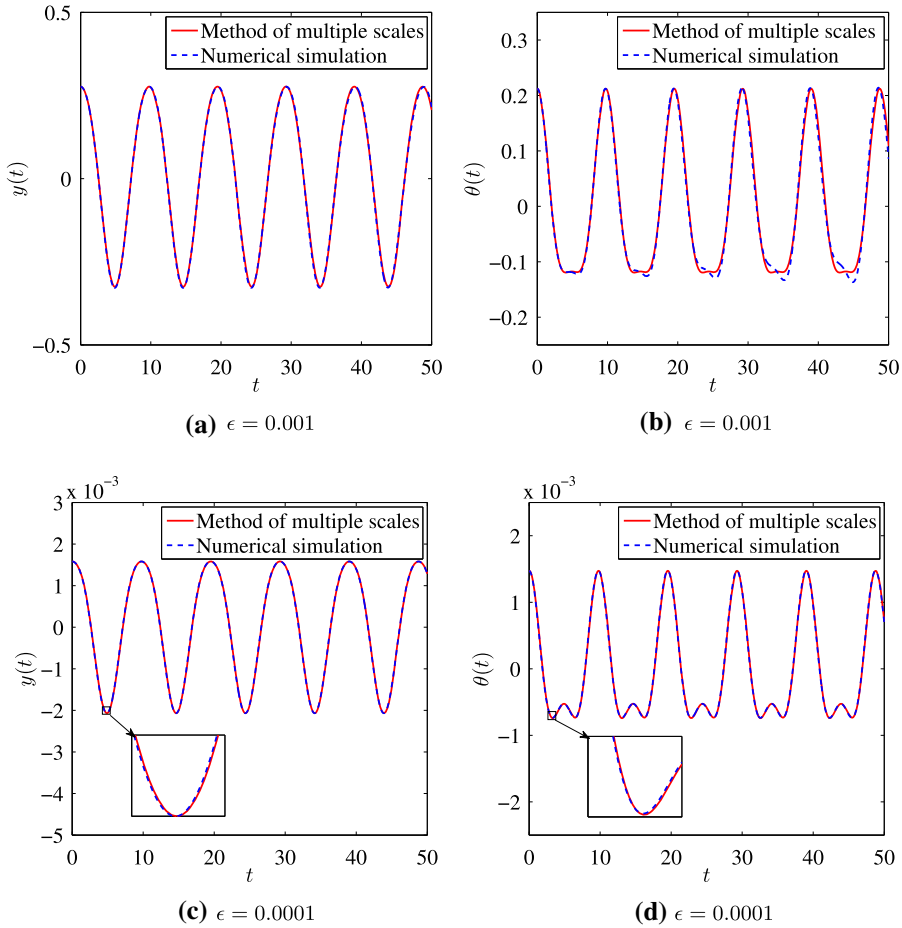

(a) $\epsilon = 0.001$ **(b)** $\epsilon = 0.001$

(c) $\epsilon = 0.0001$ **(d)** $\epsilon = 0.0001$

Fig. 4 Comparison between the numerical and analytical solutions for the system parameters given in Table 1 **(a)**, **(c)**, translational motion, $y(t)$ and **(b)**, **(d)**, rocking motion, $\theta(t)$ with different values of ϵ ($\epsilon = 0.001, 0.0001$) for primary resonance near ω_1, i.e., $\omega_r = \omega_1 + 0.1\epsilon$, and $f_0 = 1$ with $1:2$ complete internal resonance, i.e., $\sigma_2 = 0$

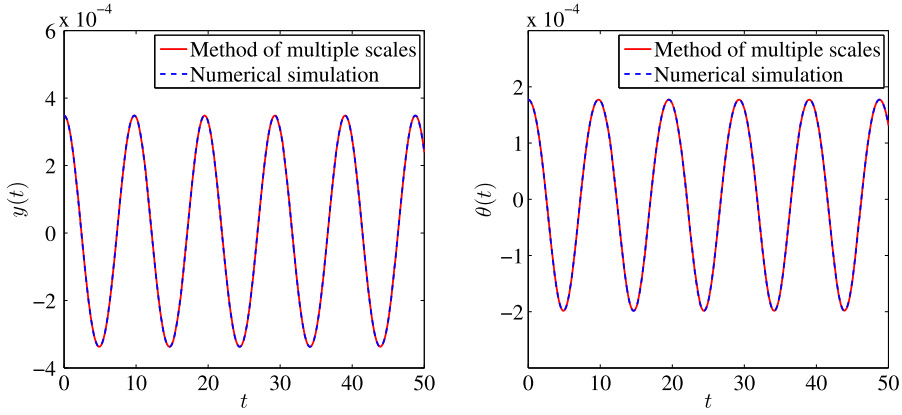

(a) **(b)**

Fig. 5 Comparison between the numerical and analytical solutions for the system parameters given in Table 1 **(a)** translational motion, $y(t)$, and **(b)** rocking motion, $\theta(t)$ for primary resonance near ω_2, i.e., $\omega_r \approx \omega_2 + 0.1\epsilon$, $\epsilon = 0.0001$ and $f_0 = 1$ with $1:2$ complete internal resonance, i.e., $\sigma_2 = 0$

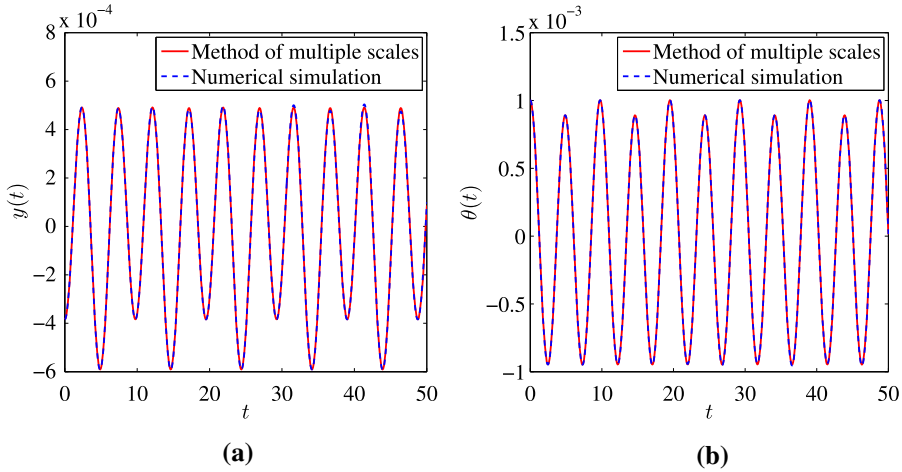

Fig. 6 Comparison between the numerical and analytical solutions for the system parameters given in Table 1 **(a)** translational motion, $y(t)$, and **(b)** rocking motion, $\theta(t)$ for superharmonic resonance near ω_1, i.e., $2\omega_r \approx \omega_1 + 0.1\epsilon$, $\epsilon = 0.0001$ and $f_0 = 1$ with $1:2$ internal resonance, i.e., $\sigma_2 = 0$

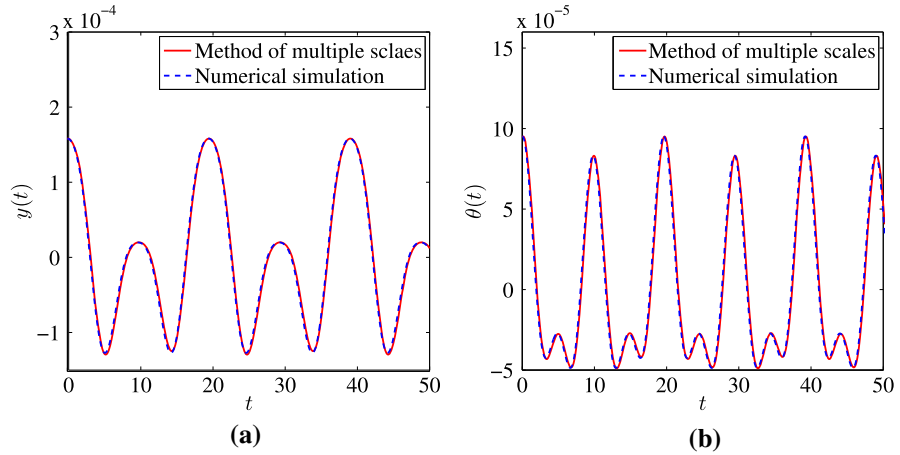

Fig. 7 Comparison between the numerical and analytical solutions for the system parameters given in Table 1 **(a)** translational motion, $y(t)$, and **(b)** rocking motion, $\theta(t)$ for superharmonic resonance near ω_2, i.e., $2\omega_r \approx \omega_2 + 0.1\epsilon$, $\epsilon = 0.0001$ and $f_0 = 4$ with $1:2$ internal resonance, i.e., $\sigma_2 = 0$

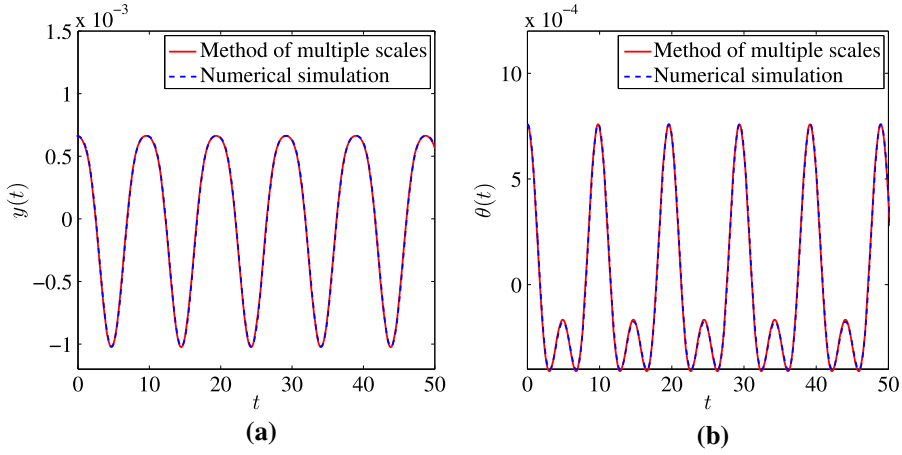

Fig. 8 Comparison between the analytical and numerical simulations for the given system parameters in Table 1 **(a)**, translational motion, $y(t)$ and **(b)** rocking motion, $\theta(t)$ for combined resonance, i.e., $\omega_r \approx \omega_1 + \omega_2 + 0.1\epsilon$, $\epsilon = 0.0001$ and $f_0 = 1$ with $1:2$ internal resonance, i.e., $\sigma_2 = 0$

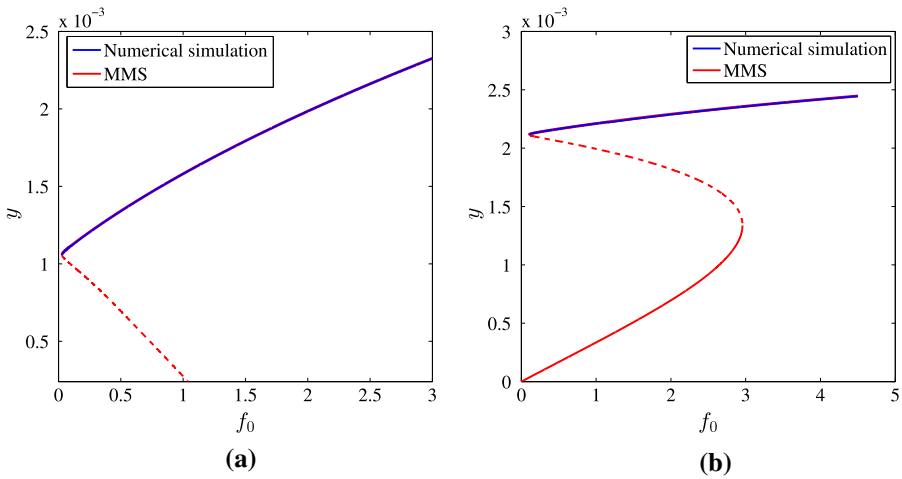

Fig. 9 comparison between numerical and analytical force response curves for the case of primary resonance near **(a)** ω_1 ($\omega_r = \omega_1 + 0.1\epsilon$), and **(b)** ω_2 ($\omega_r = \omega_2 + 0.1\epsilon$) with $1:2$ internal resonance, i.e., $\sigma_2 = 0$

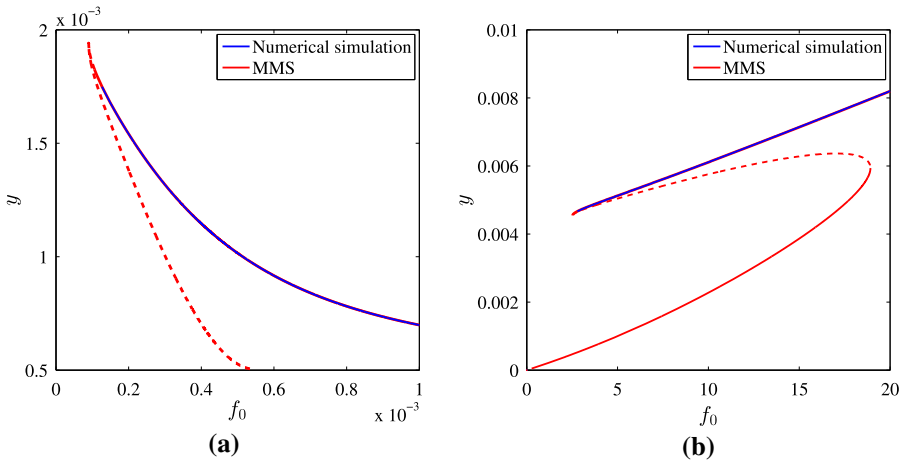

Fig. 10 Comparison between numerical and analytical force response curves for the case of superharmonic resonance near **(a)** ω_1 ($2\omega_r = \omega_1 + 0.1\epsilon$), and **(b)** ω_2 ($2\omega_r = \omega_2 + 0.1\epsilon$) with $1:2$ internal resonance, i.e., $\sigma_2 = 0$

force response curves of the first and second modes corresponding to primary resonance are shown in Fig. 12 for different values of external detuning parameter σ_1. From Fig. 12a, we can observe that for the case of a small value of detuning in the external excitation and perfectly internal tuned system, there are different solutions in different regions of the excitation amplitude. From Fig 12a, it can be observed that in the region $f_{01} < f_0 < f_{02}$, three simultaneous solutions exist for mode a_2 (Eqs. (24) and (25)). The stability of these steady-state solutions can be accessed by calculating the eigenvalues of the Jacobian matrix corresponding to primary resonance near ω_1. The unstable and stable branches of the solution are shown by dashed and solid lines, respectively. It is noted that two out of three solutions are stable, and one branch of steady solution ($a_2^* = 0$) becomes unstable as the excitation amplitude increases beyond f_{02}. Further, from Fig. 12a, it can be observed that two unstable branches of the solution merge with one stable branch of the solution at f_{02} and produce one unstable branch for mode a_2. This observation leads to a subcritical mode bifurcation in the system for mode a_2. Accordingly, the initial conditions, close to the stable solutions, determine the response of the system in this region, which further implies the local stability of the dynamical system for $f_{01} < f_0 < f_{02}$. However, for the case of zero detuning in the external excitation and perfectly tuned internal resonance system, only one solution of the steady state, i.e., $a_2 = 0$, exists for $f_0 < f_{02}$ and two solutions of steady state exist for $f_0 > f_{02}$. On accessing the stability of these steady states, it can be observed that $a_2 = 0$ becomes unstable as f_0 increases after f_{02}. This observation further implies that two stable and one unstable branches of the solution emerge at $f_0 = f_{01}$, leading to a supercritical mode bifurcation in the system.

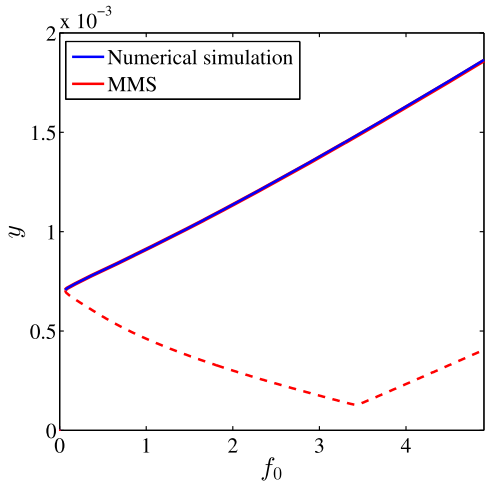

Fig. 11 Comparison between numerical and analytical force response curves for the case of combined resonance $\omega_r = \omega_1 + \omega_2 + 0.1\epsilon)$ with $1:2$ internal resonance, i.e., $\sigma_2 = 0$

Further, the saturation phenomenon in mode a_1 can be observed for both cases of external detuning. From Figs. 12a and 12b, it can be observed that as f_0 increases, a_1 increases while a_2 remains unexcited regardless of the value of detuning parameter. However, as the value of external excitation, f_0, reaches a critical value of f_{02}, there is no further increment in the value of a_1, and it gets saturated. After this value of f_0, increment in the external excitation only causes growth in a_2. This observation further suggests that there is no energy exchange between the modes for the case of primary resonance near ω_1.

On analyzing the case of superharmonic resonance near ω_1, we notice that observations similar to the primary resonance case can also be drawn for this case. These qualitative similarities between the primary and superharmonic resonance near ω_1 exist because of the similar form for the steady-state values in both of the

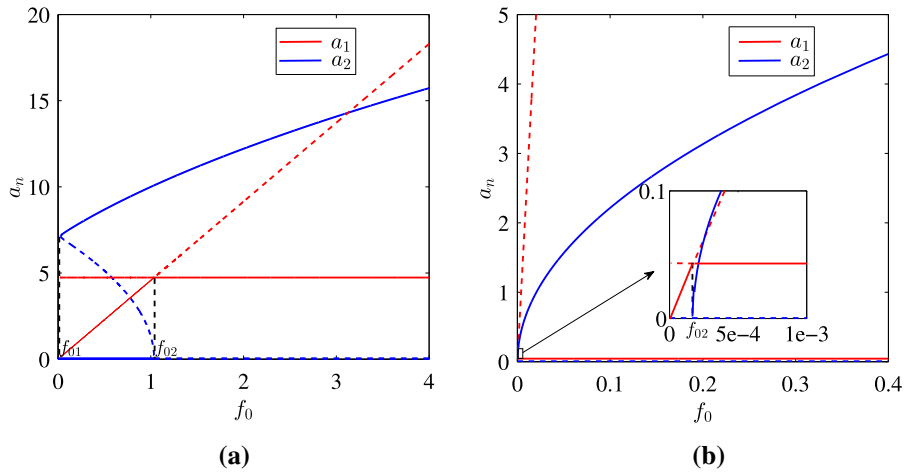

Fig. 12 Force response curve of the first and second modes, i.e., a_1 and a_2 for primary resonance near ω_1 with **(a)** $\omega_r = \omega_1 + 0.1\epsilon$, $\epsilon = 0.0001$; **(b)** $\omega_r = \omega_1$ and $1:2$ internal resonance, i.e., $\sigma_2 = 0$

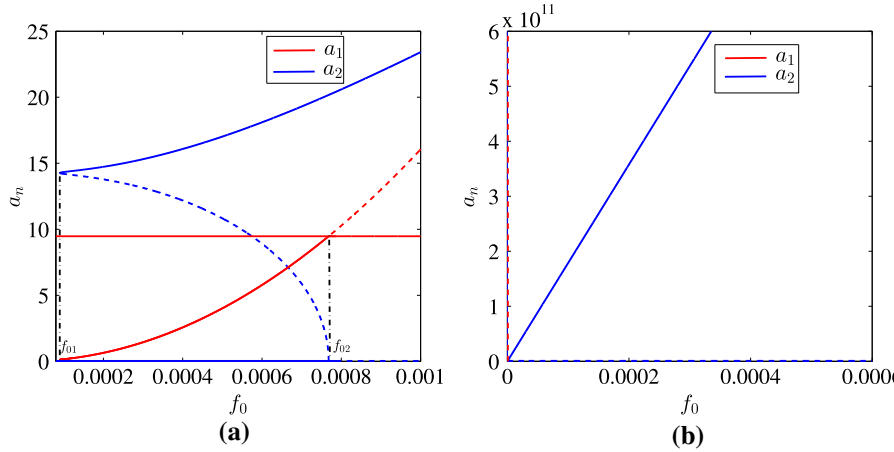

Fig. 13 Force response curve of the first and second modes, i.e., a_1 and a_2 for superharmonic resonance with **(a)** $2\omega_r = \omega_1 + 0.1\epsilon$, $\epsilon = 0.0001$; **(b)** $2\omega_r = \omega_1$ and $1:2$ internal resonance, i.e., $\sigma_2 = 0$

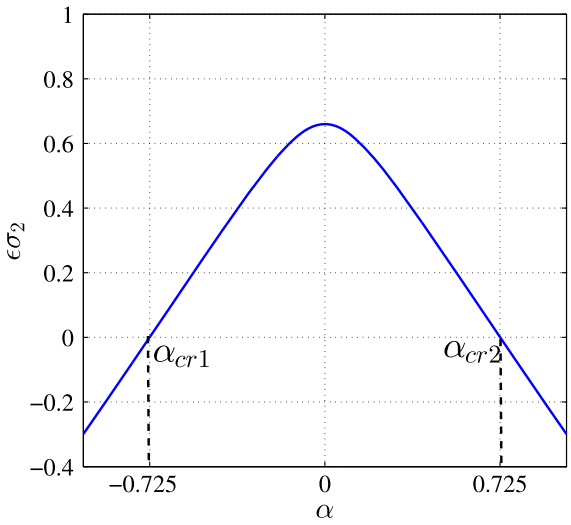

Fig. 14 Variation in internal detuning parameter with nondimensional location of the isolator for the values of system parameters given in Table 1

cases. However, it can be noticed from Fig. 13b that for the case of zero detuning in external excitation, the response of the system is governed by the mode a_2 only and attains a very high value for the given excitation. The latter indicates that nonlinear interaction can be employed in transferring the energy to one of the modes (i.e., the translation or rocking) with isolating other unwanted motions that affect the performance of UPM machines.

Next, we present the effect of isolator location on the nature of bifurcation through internal detuning parameter σ_2. For this, it is required to know the variation in internal detuning parameter with isolator location (α) and hence is shown in Fig 14. It can be observed from this figure that perfect internal resonance (i.e., $\sigma_2 = 0$) occurs when $\alpha = \alpha_{cr1}$ (-0.725) or $\alpha = \alpha_{cr2}$ (0.725). Negative detuning occurs when $\alpha < \alpha_{cr1}$ or $\alpha > \alpha_{cr2}$, whereas positive detuning occurs when $\alpha_{cr1} < \alpha < \alpha_{cr2}$. The system is uncoupled when $\alpha = 0$ and this corresponds to positive detuning (i.e., $\sigma_2 \approx 0.65$). The role of the isolator location on the bifurcation of the system is demonstrated in Figs. 15 and 16 for the primary and superharmonic resonance, respectively.

From Fig. 15, it can be noted that for the case of primary resonance, there is a change in the nature of bifurcation from supercritical to subcritical as the internal detuning parameter becomes negative from positive. Since the internal detuning parameter is related to the location of isolators through the natural frequencies, the nature of bifurcation and hence the stable global region depend on the location of isolators. Further, from Fig. 14 we can observe that for $\alpha = 0$ (i.e., for completely decoupled system) internal detuning parameter remains positive which signifies the existence of supercritical bifurcation and global stable region. This observation is in contrary to the findings in [34] where it was shown that mode coupling is always desirable for better vibration suppression. However, from Fig. 16 it can be noted that the above observations do not hold any longer for the case of superharmonic resonance near ω_1. We observe that for both cases of internal detuning parameter σ_2 ($\sigma_2 > 0$ and $\sigma_2 < 0$), there is no change in the nature of bifurcation as it remains subcritical. Further, for the case of superharmonic resonance with the positive value of internal detuning parameter, i.e., $\sigma_2 > 0$, the local stable region is smaller as compared to the negative value of σ_2. Although we can observe that for the same value of external excitation, the amplitude of both modes (a_1 and a_2) are much larger for the negative value of σ_2 for both cases of resonances. This observation further suggests the isolator locations, which correspond to the negative value of the internal detuning parameter should be avoided for both cases of resonance near ω_1.

Now, we present the resonance cases close to the lower natural frequency of the system, i.e., ω_2. The force response curves of the first and second modes corresponding to primary and superharmonic resonance near ω_2 are shown in Figs. 17 and 18, respectively, for different values of external detuning parameter σ_1. From Figs. 17a and 18a, it can be observed that with the small value of detuning in the external excitation frequency and perfectly internal tuned system, there are different solutions in the different regions of the excitation amplitude. From Figs. 17a and 18a, we observe the existence of S-shaped bifurcation [45] with two turning points and three simultaneous solutions for both modes a_1 and a_2 in the region of $f_{01} < f_0 < f_{02}$. The stability of these steady- state solutions can be accessed by calculating the eigenvalues of the Jacobian matrix corresponding to the primary and superharmonic resonance near ω_2. Again, the unstable and stable branches of the solution are shown by dashed and solid lines, respectively. It is noted that two out of three solutions in the region $f_{01} < f_0 < f_{02}$ are stable. Further, we note that for smaller excitation amplitude $f_0 \in (0, f_{02})$, the

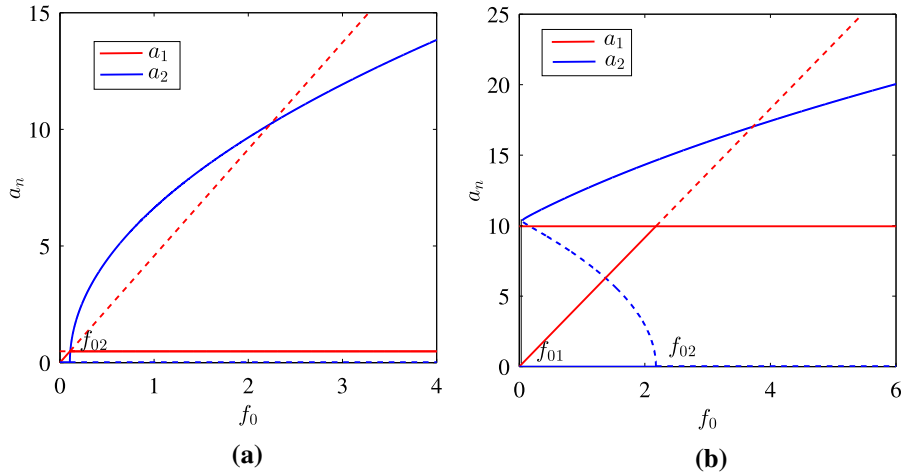

Fig. 15 Force response curve for the case of primary resonance with $\sigma_1 = 0.1$, $\epsilon = 0.0001$ **(a)** $\sigma_2 = 0.11$, and **(b)** $\sigma_2 = -0.11$

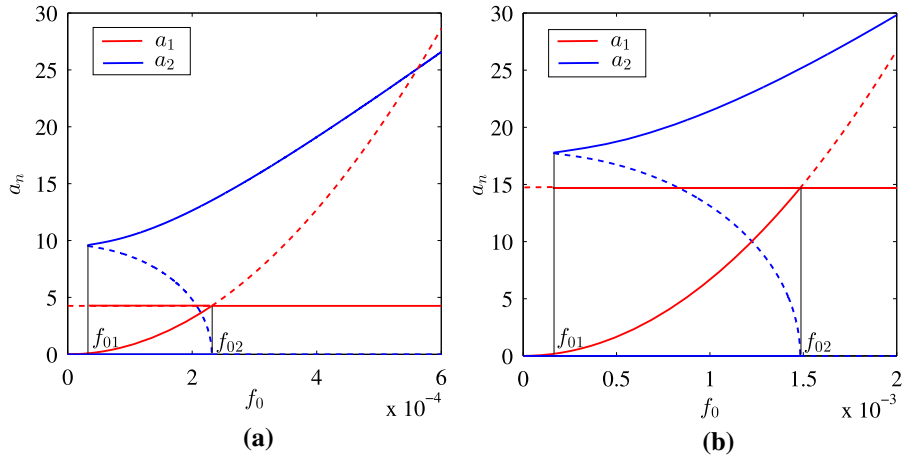

Fig. 16 Force response curve for the case of superharmonic resonance with $\sigma_1 = 0.1$, $\epsilon = 0.0001$ **(a)** $\sigma_2 = 0.11$, and **(b)** $\sigma_2 = -0.11$

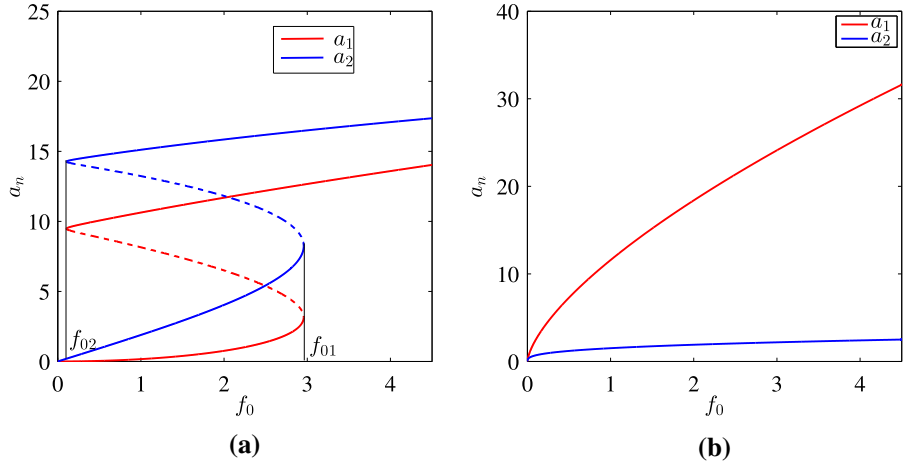

Fig. 17 Force response curve of the first and second modes, i.e., a_1 and a_2 for primary resonance near ω_2 with **(a)** $\omega_r = \omega_2 + 0.1\epsilon$, $\epsilon = 0.0001$; **(b)** $\omega_r = \omega_2$ and $1:2$ internal resonance, i.e., $\sigma_2 = 0$

amplitude of both modes a_1 and a_2 attains very small values, irrespective of the initial conditions. However, between f_{02} and f_{01}, the stability of the steady states results in conditional persistence.

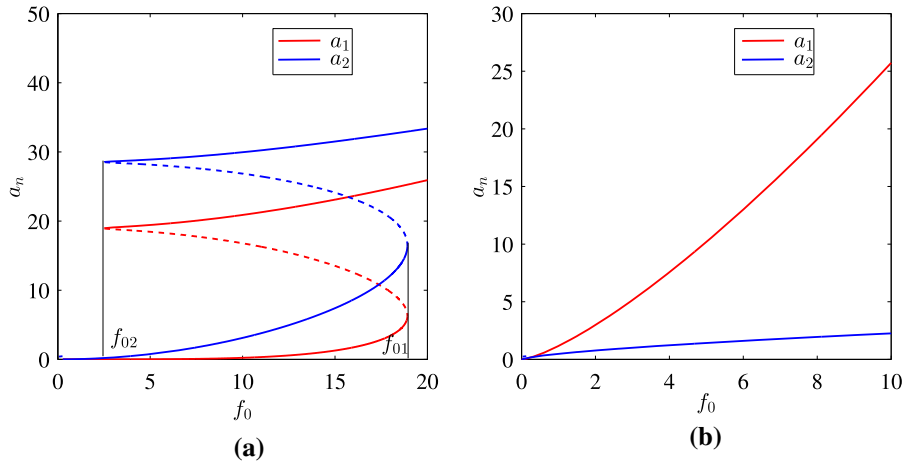

Fig. 18 Force response curve of the first and second modes, i.e., a_1 and a_2 for superharmonic resonance near ω_2 with **(a)** $2\omega_r = \omega_2 + 0.1\epsilon$, $\epsilon = 0.0001$; **(b)** $2\omega_r = \omega_2$ and $1:2$ internal resonance, i.e., $\sigma_2 = 0$

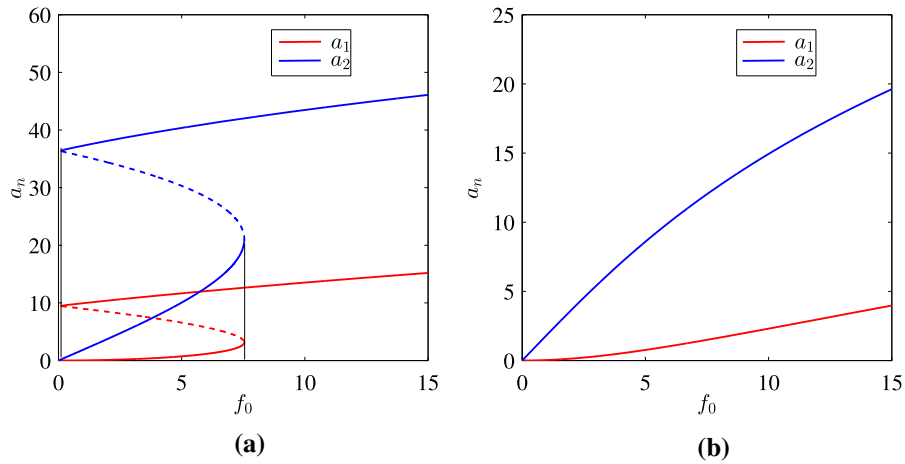

Fig. 19 Force response curve for the case of primary resonance near ω_2 with $\sigma_1 = 0.1$, $\epsilon = 1e-4$ **(a)** $\sigma_2 = 0.11$, and **(b)** $\sigma_2 = -0.11$

In this range, the top and bottom branches are stable solutions while the middle branch is unstable. Thus, the amplitude of both modes is highly dependent on initial conditions. For example, if the initial conditions corresponds to the values on the lower side of the middle branch, the amplitude will decrease until it reaches the stability at the lower branch, whereas, with initial conditions corresponding to upper side of middle branch, amplitude will increase until obtaining stability at the top branch. For $f_0 > f_{01}$, the amplitude of both modes will unconditionally persist. It implies that with any combination of initial conditions, the amplitude will increase or decrease until stabilizing at the top branch. However, for the case of exact external resonance, i.e., $\sigma_1 = 0$, there is only one stable solution (Figs. 17b and 18b) for both cases of resonance, irrespective of the value of f_0. This further implies that both modes achieve the steady state irrespective of the initial conditions. Further, from Figs. 17b and 18b we can observe that for the case of exact external resonance, mode a_1 dominates the dynamics of system unlike the case of resonance near ω_1 where a_2 was the dominant mode. Also, we observe that there is no saturation phenomenon of any of the modes unlike the resonance cases near ω_1. This observation further implies the continuous energy exchange between both modes a_1 and a_2.

Now, we present the effect of isolator location on the force response of the system through internal detuning parameter σ_2. From Fig. 19 we can observe that for the case of primary resonance near ω_2, there is change in the nature of force response curve with the change in the sign of internal detuning parameter σ_2. However, from Fig. 20 we again note that the above observation does not hold any longer for the case of superharmonic resonance near ω_2 like the case of resonances near ω_1.

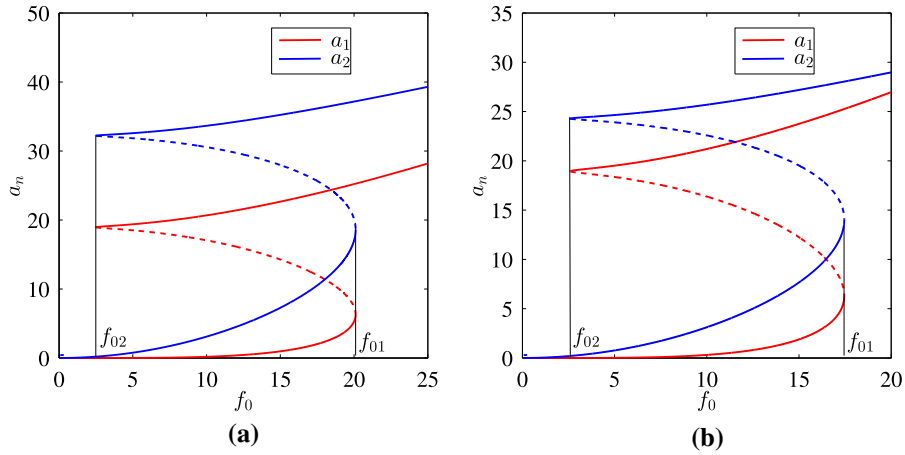

Fig. 20 Force response curve for the case of superharmonic resonance near ω_2 with $\sigma_1 = 0.1$, $\epsilon = 1e-4$ **(a)** $\sigma_2 = 0.11$, and **(b)** $\sigma_2 = -0.11$

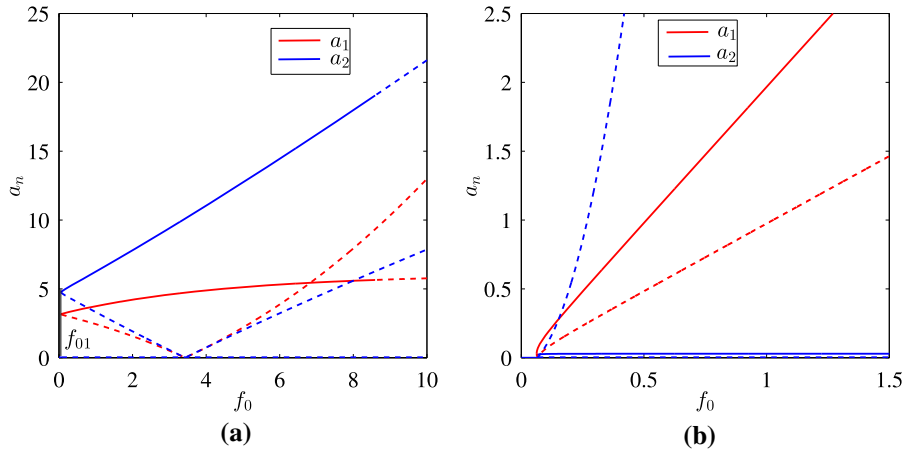

Fig. 21 Force response curve of the first and second modes, i.e., a_1 and a_2 for combined resonance with **(a)** $\omega_r = \omega_1 + \omega_2 + 0.1\epsilon$, $\epsilon = 0.0001$; **(b)** $\omega_r = \omega_1 + \omega_2$ and $1:2$ internal resonance, i.e., $\sigma_2 = 0$

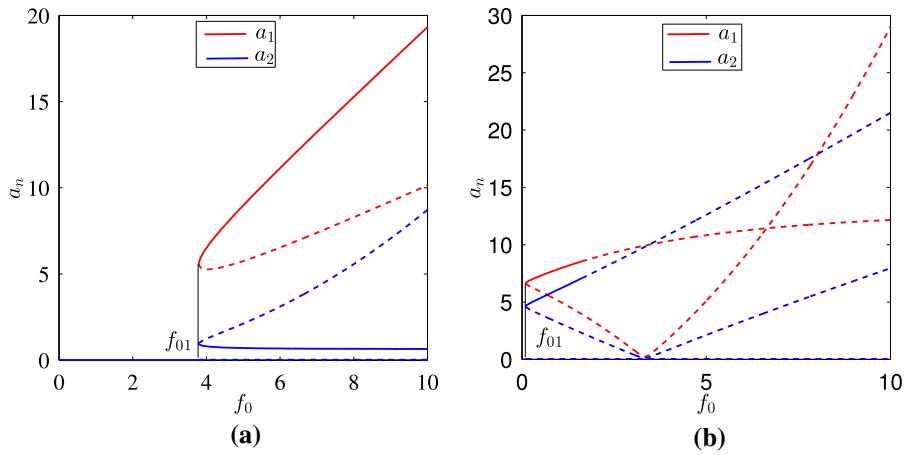

Fig. 22 Force response curve for the case of combined resonance with $\sigma_1 = 0.1$, $\epsilon = 1e-4$ **(a)** $\sigma_2 = 0.11$, and **(b)** $\sigma_2 = -0.11$

Also, for the case of superharmonic resonance near ω_2, with positive value of internal detuning parameter, i.e., $\sigma_2 > 0$, the unstable branch of solution is larger as compared to negative value of σ_2. Note that this observation is in contrast with the case of resonance near ω_1, where positive value of external detuning causes small local stable region. Furthermore, we observe that for the same value of excitation, amplitude of modes, a_1 and a_2 are much larger for positive value of σ_2 unlike the case of resonance near ω_1. This observation fur-

ther suggests the isolator location which corresponds to the positive value of internal detuning parameter, σ_2, should be avoided for the case of resonances near ω_2.

The force response curves for the case of combined resonance are shown in Figs. 21 and 22 for the different values of σ_1 and σ_2. From these figures, it can be observed that f_0 should be greater than the critical value f_{01} to change the steady states from zero to nonzero values. After this value of excitation, amplitudes $a_1 = 0$ and $a_2 = 0$ become unstable. The unstable and stable branches of the solutions are shown using the solid and dashed lines, respectively. We note that for the different combination of σ_1 and σ_2, the amplitude of first mode changes very slowly after a certain value of excitation amplitude as compared to the second mode. This saturation phenomenon of mode a_1 can be referred to as quasi-saturation and happens at high value of excitation amplitude. Finally, we also observe that for larger f_0, all the steady states become unstable.

Next we present the frequency response of the system for different cases of resonance. The frequency response curves for modes a_1 and a_2 corresponding to primary and superharmonic resonance near ω_1 are shown in Figs. 23 and 24. The dotted curves for a_1 with peaks at $\sigma_1 = 0$ correspond to steady state $a_2^* = 0$ and essentially are the solution of the corresponding linear problem. It can be observed that unstable region for the linear solution depends on the value of σ_1 and the solution corresponding to the nonlinear system. Also, from these figures, it can be observed that for both cases, primary and secondary resonance, nonlinearity in the system is primarily depicted by mode a_2. Therefore, for the remainder of the analysis we consider mode a_2 only.

The frequency response curves for primary and superharmonic resonance near ω_2 are shown in Figs. 25 and 26. We observe that near the value of zero external detuning parameter, the amplitude of mode a_2 is smaller than a_1. However, as the value of σ_1 increases, the amplitude of mode a_2 becomes dominant and attains a higher value as compared to a_1 for the given σ_2. Further, we observe the jump phenomenon like the earlier cases of resonance.

The frequency response for the combined resonance is shown in Fig. 27. We observed that for the values of σ_1 close to 0, both trivial and nontrivial steady states are unstable. To further analyze the system, we present the effect of different parameters on the system dynamics.

6 Effect of parameters on the system dynamics

In this section, we present the effect of different system parameters on the dynamics of the system in order to identify the key design parameters. As discussed earlier, the effect of nonlinearity in the system is more prominent in mode a_2. We plotted the frequency response curve for mode a_2 for different values of system parameters corresponding to primary and superharmonic resonance. In Fig. 28a, the effect of β, ratio of natural frequency corresponding to uncoupled translational and rocking motion, on the frequency response is shown. From these frequency response curves, we can observe that with the increase in β, the maximum amplitude of a_2 and the effect of nonlinearity increases significantly . Also, the unstable region corresponding to $a_2 = 0$ increases with increasing β. However, it should be noted here that parameter β is not associated directly with any nonlinear terms in the system of equations (Eq. (5)). This observation further motivates the importance of linear and nonlinear mode coupling in the system. Figure 28b depicts the effect of k_r on the system dynamics. It is demonstrated that with the increase in the value of k_r, ratio of linear stiffnesses corresponding to equivalent isolator in translational and rocking direction has little effect on the dynamics of modal amplitude. Moreover, one can observe that the rate of change of the backbone curve and amplitude with respect to k_r is very low and a higher value of k_r is required to decrease the amplitude. The effect of variation in q_{zr}, representing the nonlinear quadratic stiffness for rocking motion, on the system dynamics is depicted in Fig 28c. It can be noted that with the increase in q_{zr}, the maximum amplitude of a_2 remains the same; however, the nonlinearity in the system increases. Also, increase in q_{zr} increases the unstable region near $\sigma_1 = 0$. Figure 28d shows the effect of α_1, representing the nondimensional quadratic stiffness for the translational motion, on the frequency amplitude characteristic. We observe that with the increase in α_1, the nonlinearity decreases while the maximum amplitude remains almost the same, unlike the other system parameters and similarly to q_{zr}. From these observations, we can easily conclude that lower value of β causes low amplitude of a_2 and further low amplitude of vibrations in the system for primary resonance.

The effect of variation of system parameters on the dynamics of the isolated UPM machine for the case of superharmonic resonance is plotted in Fig. 29. The

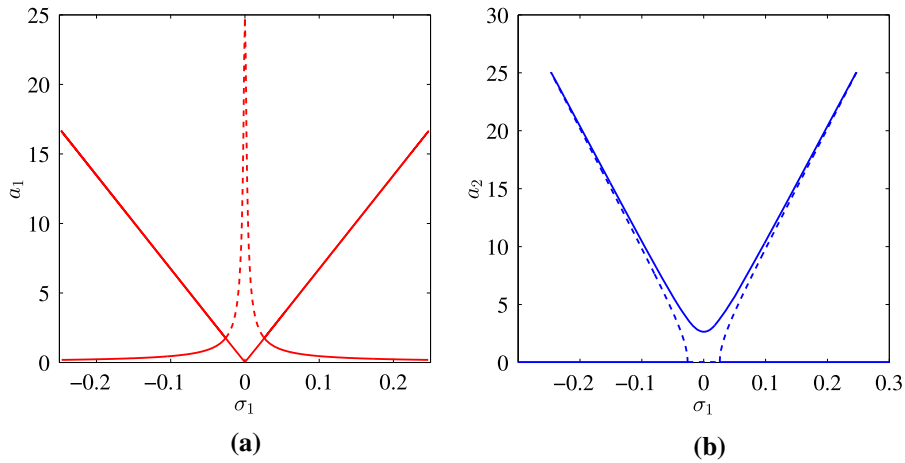

Fig. 23 Frequency response curve for primary resonance **(a)** first mode; **(b)** second mode with $f_0 = 0.1$, $\epsilon = 0.0001$, and $1:2$ perfect internal resonance, i.e., $\sigma_2 = 0$

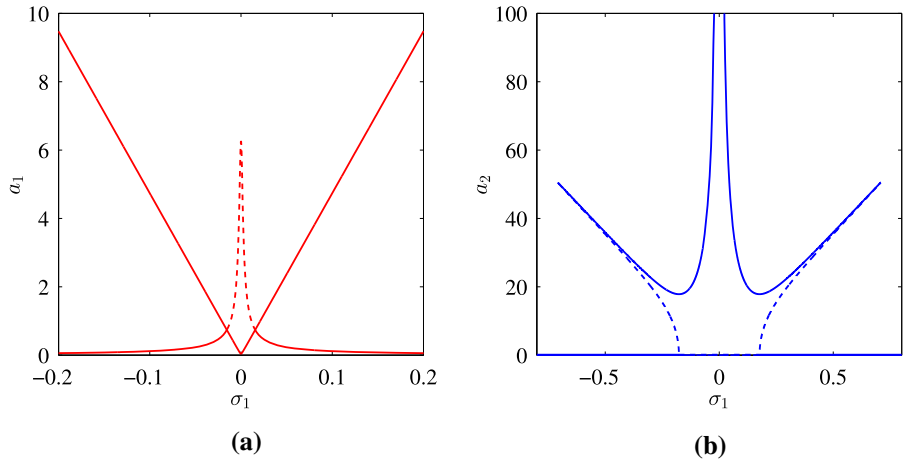

Fig. 24 Frequency response curve for superharmonic resonance **(a)** first mode; **(b)** second mode with $f_0 = 6e - 4$, $\epsilon = 0.0001$ and $1:2$ perfect internal resonance, i.e., $\sigma_2 = 0$

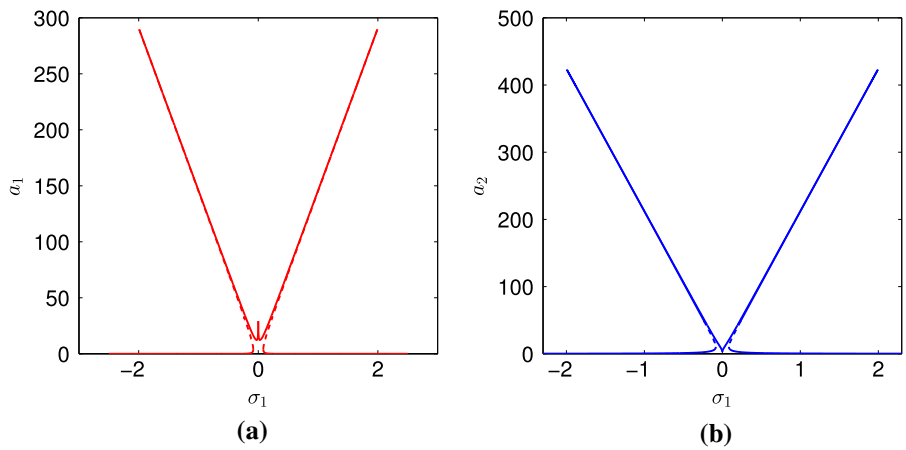

Fig. 25 Frequency response curve for primary resonance near ω_2 **(a)** first mode; **(b)** second mode with $f_0 = 3$, $\epsilon = 0.0001$ and $1:2$ perfect internal resonance, i.e., $\sigma_2 = 0$

results show that with increasing β, there is an increase in the nonlinearity in the system similar to the case of primary resonance. However, the maximum amplitude for a_2 decreases significantly with small increase in β. The effect of variation in k_r is shown in Fig. 29b. From this figure, it can be easily observed that k_r does not significantly influence the nonlinearity of the system, like in the case of primary resonance. Figure 29c

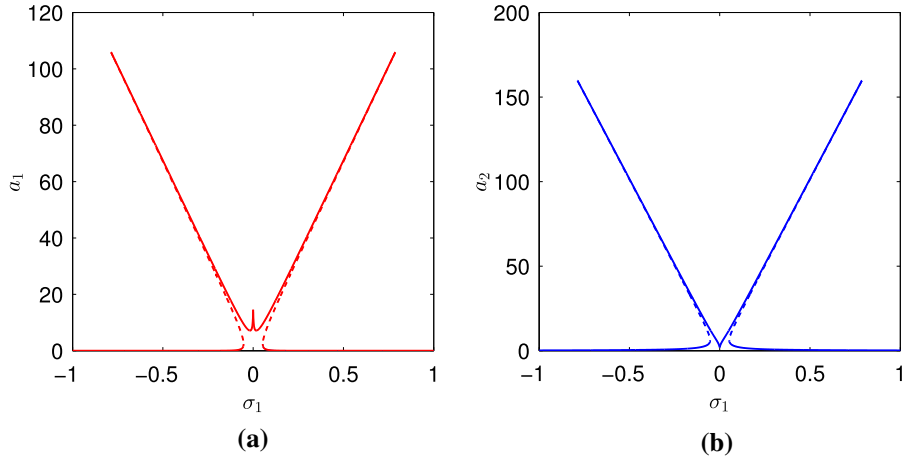

Fig. 26 Frequency response curve for superharmonic resonance **(a)** first mode; **(b)** second mode with $f_0 = 6$, $\epsilon = 0.0001$ and $1:2$ perfect internal resonance, i.e., $\sigma_2 = 0$

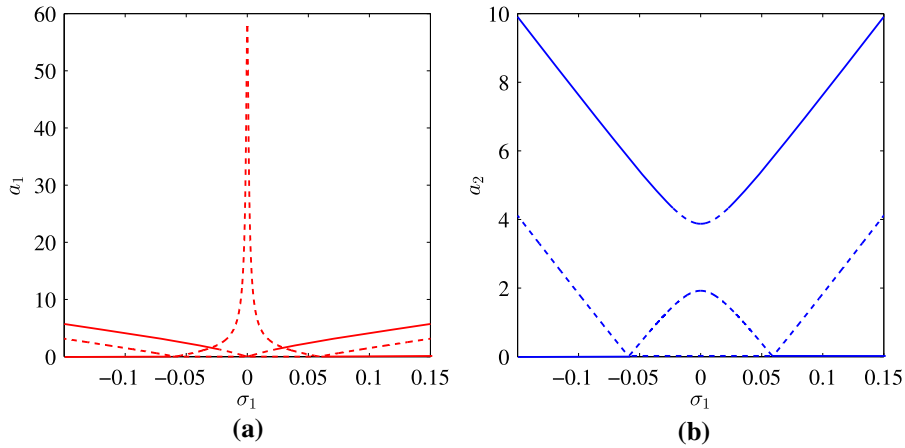

Fig. 27 Frequency response curve for superharmonic resonance **(a)** first mode; **(b)** second mode with $f_0 = 6$, $\epsilon = 0.0001$ and $1:2$ perfect internal resonance, i.e., $\sigma_2 = 0$

shows the variation in frequency response curves with q_{zr}. Increasing q_{zr} does not only decrease the maximum amplitude, but also increases the nonlinearity in the system. Contrary to other parameters, nonlinearity in the system decreases with increasing α_1. However, this increment further increases the maximum amplitude. Therefore, to limit the maximum value of modal amplitude a_2 for the case of superharmonic resonance, larger value of β and q_{zr} and lower values of α_1 are required.

Next, we present the effect of variation in system parameters on the system dynamics for the cases of resonance (primary and superharmonic) near ω_2. The results are shown in Figs. 30 and 31. For the case of primary resonance near ω_2, we note that with an increase in β, the maximum amplitude decreases with increase in nonlinearity. However, increase in k_r increases the maximum amplitude and has very marginal effect on the nonlinearity. We observe that both of the above observations for β and k_r are valid for the case of superharmonic resonance near ω_2. Further, we observe that increase in q_{zr} increases the nonlinearity in the system but has no effect on the maximum amplitude. We observe that q_{zr} has similar effect for the case of superharmonic resonance near ω_1. However, contrary to other system parameters, increase in α_1 decreases the nonlinearity in the system.

Now, we present the effect of system parameters on the system dynamics for the case of combined resonance in Fig. 32. We observe that the nonlinearity increases and the stable region near sigma1 decreases with increasing any of the dimensionless parameters, except α_1.

For a better illustration of these results, we present the effect of increase in parameters values on the maximum amplitude and nonlinearity of system in Tables 2 and 3, respectively. From Table 2, we can observe that the effect of the parameter values on the maxi-

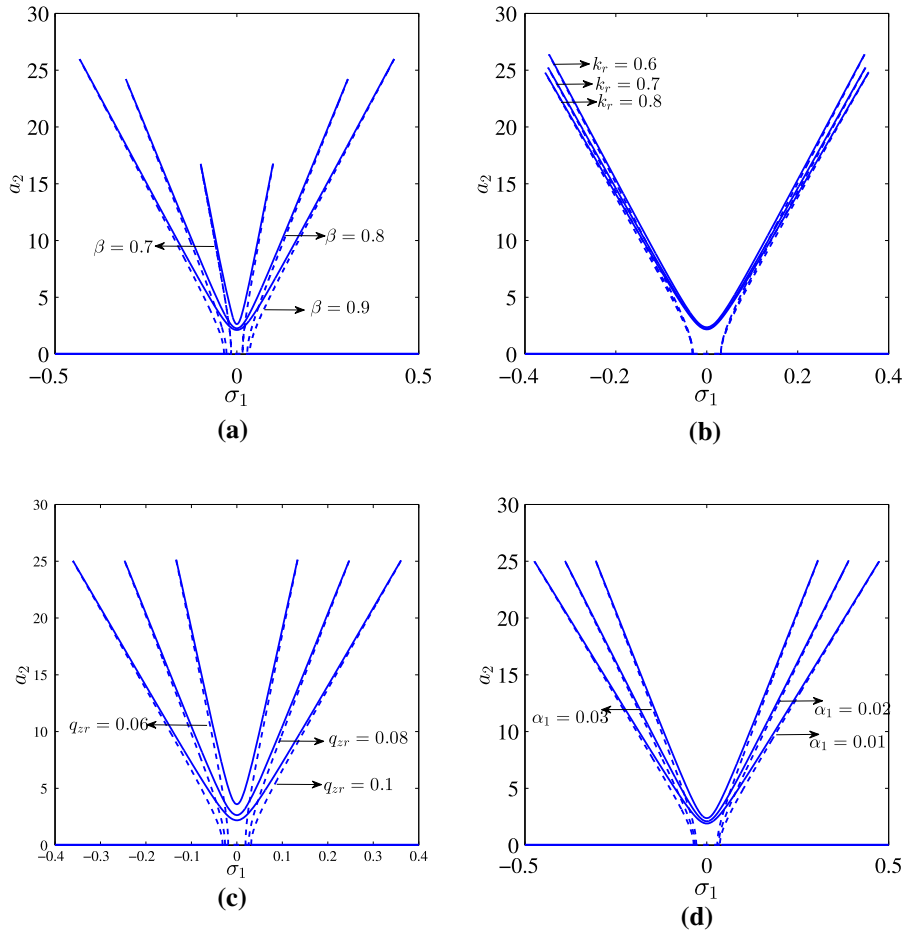

Fig. 28 Effect of variation in **a** β, **b** k_r, **c** q_{zr}, and **d** α_1 on the frequency response curves for primary resonance with $f_0 = 0.1$, $\sigma_2 = 0$ and $\epsilon = 0.0001$

mum amplitude of the system is not monotonous and changes from one case of external resonance to another. However, in contrary to these, these parameters have a consistent effect on the nonlinearity of the system, as depicted in Table 3. With these observations, we can conclude that it is not possible to decide global key design parameters which are valid for all cases of external resonance.

7 Conclusion

We studied the nonlinear vibration of a UPM machine analytically using the method of multiple scales and harmonic balance. Based on the experimental results, we assumed the stiffness of the pneumatic isolators to be a combination of linear and quadratic stiffnesses. In our mathematical formulation, the horizontal and torsional motions were also linearly and nonlinearly coupled through the location of the vibration isolators. The closed form solution for the modal amplitudes, corresponding to the different cases of external resonance with internal resonant, was obtained using MMS. The obtained analytical expressions were validated using direct numerical simulations, and the results showed very good agreement. Further analysis revealed the existence of subcritical and supercritical bifurcation for the cases of external resonance near higher natural frequencies. The results showed existence of S-shaped bifurcation for the cases of external resonance close to lower natural frequency. We also observed dependence of energy exchange between the modes for the case of external resonances. Further analysis revealed the sensitivity of the nature of bifurcation toward internal detuning parameter and hence the location of isolator. Numerical examples demonstrated that negative detuning, which corresponded to the isolator location $\alpha < \alpha_{cr1}$ or $\alpha > \alpha_{cr2}$, can degrade the performance of the isolator. Furthermore, we observed that mode

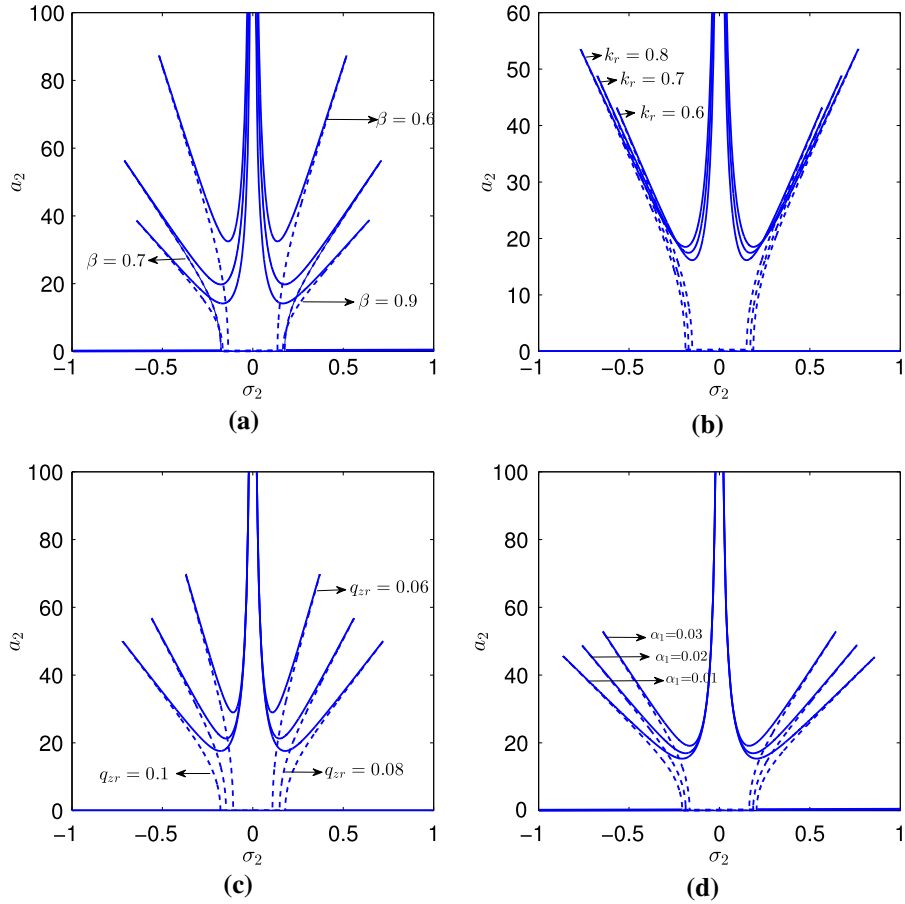

Fig. 29 Effect of variation in **a** β, **b** k_r, **c** q_{zr}, and **d** α_1 on the frequency response curves for superharmonic resonance with $f_0 = 0.1$, $\sigma_2 = 0$ and $\epsilon = 0.0001$

decoupling leads to global stable regions and hence desirable in practice in contrary to earlier studies which refuted the advantages of mode decoupling. The numerical results also showed more complicated dynamics such as quasi-saturation phenomenon for the case of combined resonance. At last, we performed the parametric study to identify key system parameters. The results showed that the effect of different parameters on the system dynamics is not monotonous and varies from one case of external resonance to another. Overall, the findings in this paper contradicted recent studies of passively isolated systems and suggested that nonlinear mode coupling can yield worst vibration isolation, especially, when the location of the vibration isolators corresponds to the internal resonance case.

Acknowledgements This work is funded by National Science Foundation (NSF) Award CMMI #2000984: Nonlinear Dynamics of Pneumatic Isolators in Ultra-Precising Manufacturing Machine.

Compliance with ethical standards

Conflict of Interest The authors declare that they have no conflict of interest.

Appendix A: primary resonance near ω_1

$$
\begin{aligned}
&D_{0,0}\eta_1 + \beta^2(\eta_1 - \alpha\vartheta_1)\\
&\quad = -2i\,(D_1A_1\Lambda_1 + A_1\zeta\beta\Lambda_1 - A_1\zeta\,\beta\,\alpha)\,\omega_1 e^{i\omega_1 T_0}\\
&\qquad - 2i\,(D_1A_2\Lambda_2 + A_2\zeta\beta\,\Lambda_2\\
&\quad -A_2\zeta\beta\alpha)\,\omega_2 e^{i\omega_2 T_0}\\
&\qquad - {A_1}^2\alpha_1 m_r\,(\alpha - \Lambda_1)^2\,e^{2i\omega_1 T_0}\\
&\qquad - {A_2}^2\alpha_1 m_r\,(\alpha - \Lambda_2)^2\,e^{2i\omega_2 T_0}\\
&\qquad - 2A_1\bar{A}_2\alpha_1 m_r\,(\alpha - \Lambda_1)\left(\alpha - \bar{\Lambda}_2\right)e^{i(\omega_1-\omega_2)T_0}\\
&\qquad + 2\,A_1A_2\alpha_1 m_r\,(\alpha - \Lambda_1)\,(\alpha - \Lambda_2)\,e^{i(\omega_1+\omega_2)T_0}\\
&\qquad + 2\,A_1\bar{A}_1\alpha_1 m_r\,(\alpha - \Lambda_1)\left(\alpha - \bar{\Lambda}_1\right)\\
&\qquad + 2A_2\bar{A}_4\alpha_1 m_r\,(\alpha - \Lambda_2)\left(\alpha - \bar{\Lambda}_2\right)\\
&\qquad + \frac{f_0}{2}m_r e^{i(\omega_1 T_0 + \sigma_1 T_1)} + C.C.\,, \qquad (56a)
\end{aligned}
$$

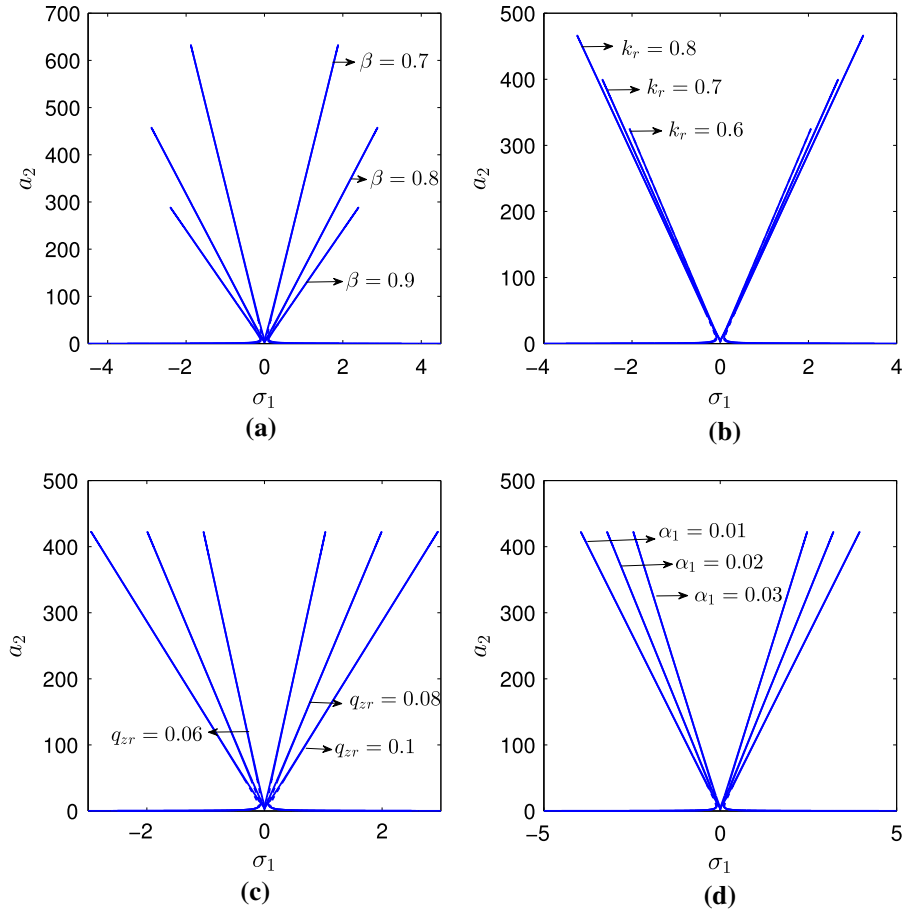

Fig. 30 Effect of variation in **a** β, **b** k_r, **c** q_{zr}, and **d** α_1 on the frequency response curves for primary resonance near ω_2 with $f_0 = 3$, $\sigma_2 = 0$ and $\epsilon = 0.0001$

Table 2 Effect of increase in parameter values on the maximum amplitude for the different cases of resonance and a given value of excitation amplitude

Cases	Parameters			
	β	k_r	q_{zr}	α_1
Primary resonance near ω_1	Increase	Decrease	No significant change	No significant change
Superharmonic resonance near ω_1	Decrease	Increase	Decrease	Increase
Primary resonance near ω_2	Decrease	Increase	No significant change	No significant change
Superharmonic resonance near ω_2	Decrease	Increase	No significant change	Decrease
Combined resonance	No effect	No effect	No effect	No effect

$$
\begin{aligned}
&D_{0,0}\vartheta_1 + \vartheta_1 - k_r\alpha\left(\eta_1 - \alpha\vartheta_1\right)\\
&\quad = -2i\omega_1\left(D_1A_1 + \sqrt{\frac{k_r}{m_r}}\zeta\alpha^2A_1\right.\\
&\qquad \left. +\kappa A_1 - \sqrt{\frac{k_r}{m_r}}\zeta\alpha A_1\Lambda_1\right)e^{i\omega_1T_0}\\
&\qquad - 2i\omega_2\left(D_1A_2 + \sqrt{\frac{k_r}{m_r}}\zeta\alpha^2A_2\right.\\
&\qquad \left. +\kappa A_2 - \sqrt{\frac{k_r}{m_r}}\zeta\alpha A_2\Lambda_2\right)e^{i\omega_2T_0}\\
&\qquad + {A_1}^2\left(\alpha_1\alpha(\alpha - \Lambda_1)^2 - q_{zr}\right)e^{2i\omega_1T_0}
\end{aligned}
$$

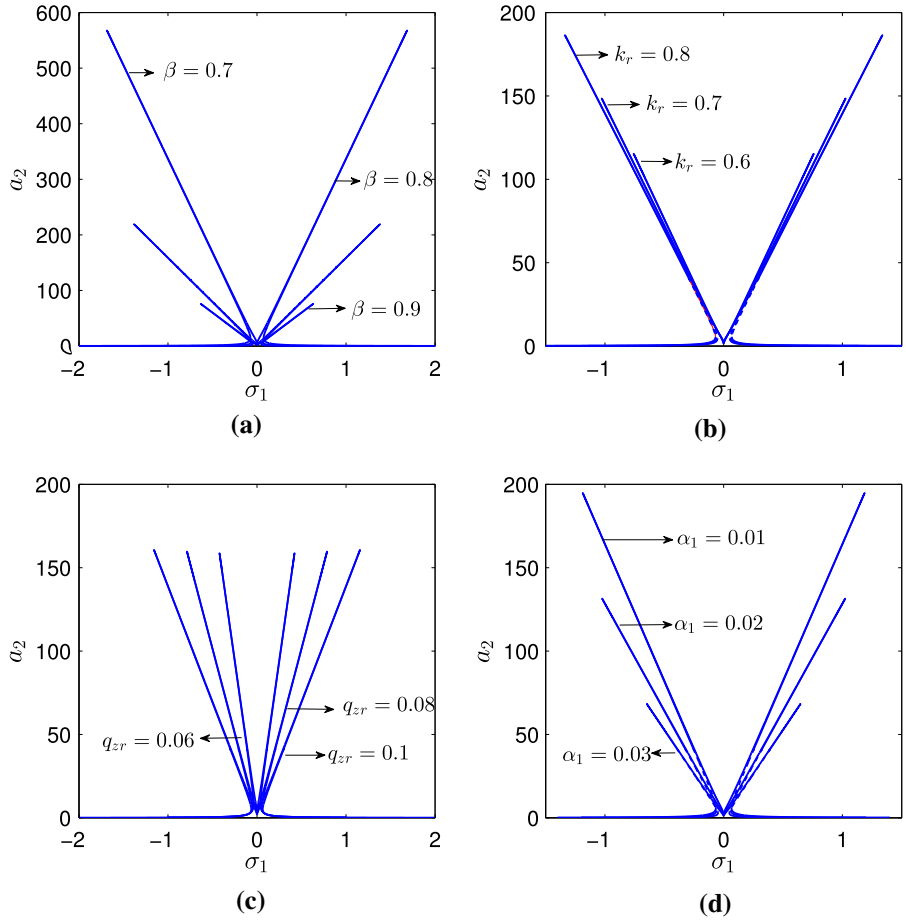

Fig. 31 Effect of variation in **a** β, **b** k_r, **c** q_{zr}, and **d** α_1 on the frequency response curves for superharmonic resonance near ω_2 with $f_0 = 6$, $\sigma_2 = 0$ and $\epsilon = 0.0001$

Table 3 Effect of increase in parameter values on the nonlinearity of the system for the different cases of resonance and a given value of excitation amplitude

Cases	Parameters			
	β	k_r	q_{zr}	α_1
Primary resonance near ω_1	Increase	Increase	Increase	Decrease
Superharmonic resonance near ω_1	Increase	Increase	Increase	Decrease
Primary resonance near ω_2	Increase	Increase	Increase	Decrease
Superharmonic resonance near ω_2	Increase	Increase	Increase	Decrease
Combined resonance	Increase	Increase	Increase	Decrease

$$
\begin{aligned}
&+ {A_2}^2 \left(\alpha_1\alpha(\alpha - \Lambda_2)^2 - q_{zr}\right) e^{2i\omega_2 T_0} \\
&+ 2A_1\bar{A}_2 \left(\alpha_1\alpha(\alpha - \Lambda_1)(\alpha - \bar{\Lambda}_2) - q_{zr}\right) e^{i(\omega_1 - \omega_2)T_0} \\
&+ 2A_1A_2 \left(\alpha_1\alpha(\alpha - \Lambda_1)(\alpha - \Lambda_2) - q_{zr}\right) e^{i(\omega_1 + \omega_2)T_0} \\
&+ 2\,A_1\bar{A}_1 \left(\alpha_1\alpha(\alpha - \Lambda_1)(\alpha - \bar{\Lambda}_1) - q_{zr}\right) \\
&+ 2\,A_2\bar{A}_2 \\
&\left(\alpha_1\alpha(\alpha - \Lambda_2)(\alpha - \bar{\Lambda}_2) - q_{zr}\right) \\
&+ \frac{f_0}{2}\alpha e^{i(\omega_1 T_0 + \sigma_1 T_1)} + C.C., \Gamma_1 \\
&= \frac{4\omega_1\zeta\left(l_1\beta - \alpha\sqrt{\frac{k_r}{m_r}}\right)(\alpha - \Lambda_1) - 4\kappa\omega_1}{4\omega_1(1 + l_1\Lambda_1)} \\
&\Gamma_2 = \frac{\alpha_1\,(\alpha - l_1 m_r)\,(\alpha - \Lambda_2)^2 - q_{zr}}{4\omega_1(1 + l_1\Lambda_1)} \\
&\Gamma_3 = \frac{2(l_1 m_r - \alpha)}{4\omega_1(1 + l_1\Lambda_1)}
\end{aligned}
$$

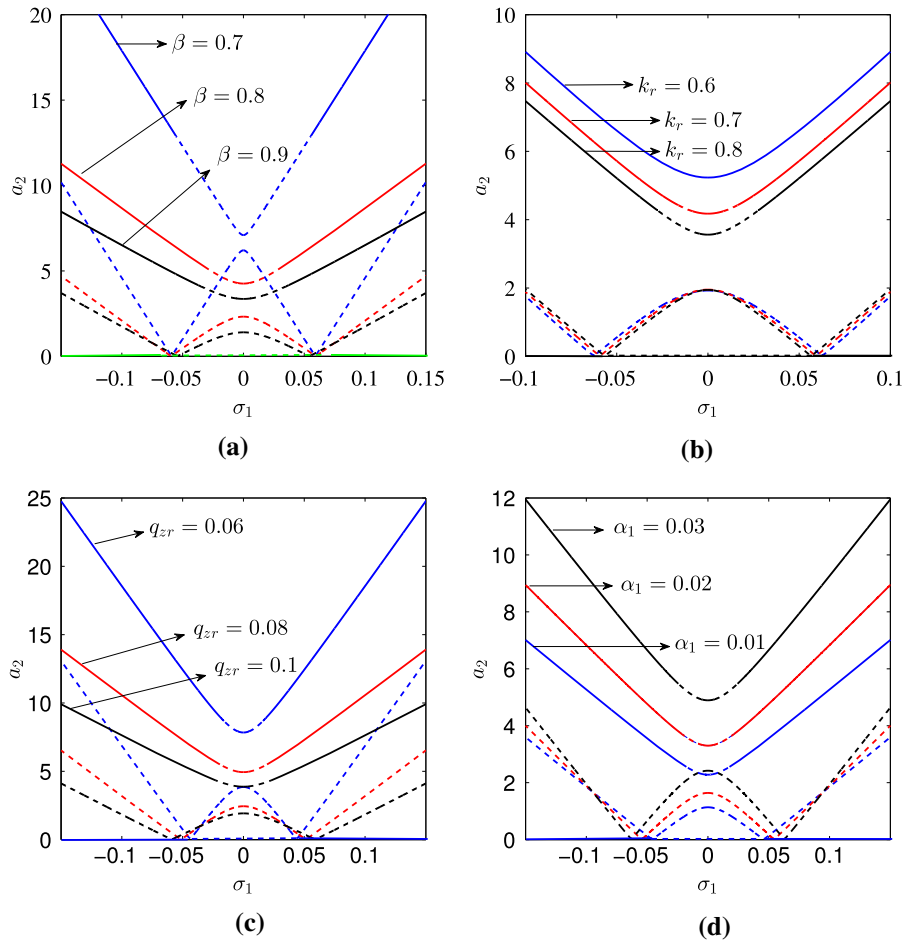

Fig. 32 Effect of variation in **a** β, **b** k_r, **c** q_{zr}, and **d** α_1 on the frequency response curves for combined resonance with $f_0 = 2$, $\sigma_2 = 0$ and $\epsilon = 0.0001$

$$\Gamma_4 = \frac{\alpha_1(l_2 m_r - \alpha)(\alpha - \bar{\Lambda}_2)(\alpha - \Lambda_1) + q_{zr}}{2\omega_2(1 + l_2\Lambda_2)}$$

$$\Gamma_5 = \frac{2\zeta\omega_2\left(l_2\beta - \alpha\sqrt{\frac{k_r}{m_r}}\right)(\alpha - \Lambda_2) - 2\kappa\omega_2}{4\omega_2(1 + l_2\Lambda_2)} \tag{56b}$$

Appendix B: primary resonance near ω_2

$$\mathcal{O}(\epsilon^0) \quad : D_{0,0}\eta_0 + \beta^2(\eta_0 - \alpha\vartheta_0) = 0\,, \tag{57a}$$

$$D_{0,0}\vartheta_0 + \vartheta_0 - k_r\alpha(\eta_0 - \alpha\vartheta_0) = 0 \tag{57b}$$

$$\begin{aligned}\mathcal{O}(\epsilon) \quad & : D_{0,0}\eta_1 + \beta^2(\eta_1 - \alpha\vartheta_1)\\ &= -2\zeta\beta(D_0\eta_0 - \alpha D_0\vartheta_0)\\ &\quad - \alpha_1 m_r(\eta_0 - \alpha\vartheta_0)^2 - 2D_{0,1}\eta_0\\ &\quad + f_0 m_r\cos(\omega_2 T_0 + \sigma_1 T_1)\end{aligned} \tag{58a}$$

$$\begin{aligned}&D_{0,0}\vartheta_1 + \vartheta_1 - k_r\alpha(\eta_1 - \alpha\vartheta_1)\\ &= 2\zeta\sqrt{\frac{k_r}{m_r}}\alpha(D_0\eta_0 - \alpha D_0\vartheta_0) - 2D_{0,1}\vartheta_0\\ &\quad + \alpha_1\alpha(\eta_0 - \alpha\vartheta_0)^2 - q_{zr}\vartheta_0^2\\ &\quad - 2\kappa D_0\vartheta_0 - f_0\alpha\cos(\omega_2 T_0 + \sigma_1 T_1)\,.\end{aligned} \tag{58b}$$

Appendix C: secondary resonance

$$\begin{aligned}&D_{0,0}\eta_1 + \beta^2(\eta_1 - \alpha\vartheta_1)\\ &\quad = -2i\left(D_1 A_1\Lambda_1 + A_1\zeta\beta\Lambda_1 - A_1\zeta\,\beta\,\alpha\right)\omega_1 e^{i\omega_1 T_0}\\ &\quad\quad - 2i\left(D_1 A_2\Lambda_2 + A_2\zeta\beta\,\Lambda_2 - A_2\zeta\beta\alpha\right)\omega_2 e^{i\omega_2 T_0}\\ &\quad\quad - {A_1}^2\alpha_1 m_r(\alpha - \Lambda_1)^2 e^{2i\omega_1 T_0} - {A_2}^2\alpha_1 m_r\\ &\quad\quad (\alpha - \Lambda_2)^2 e^{2i\omega_2 T_0}\\ &\quad\quad - 2A_1\bar{A}_2\alpha_1 m_r(\alpha - \Lambda_1)\left(\alpha - \bar{\Lambda}_2\right)e^{i(\omega_1 - \omega_2)T_0}\\ &\quad\quad + 2\,A_1 A_2\alpha_1 m_r(\alpha - \Lambda_1)(\alpha - \Lambda_2)\,e^{i(\omega_1 + \omega_2)T_0}\\ &\quad\quad + A_1\alpha_1 m_r f_0(\alpha - \Lambda_1)(\Phi_1 - \alpha\Phi_2)\,e^{i(\omega_1 - \omega_r)T_0}\\ &\quad\quad + A_1\alpha_1 m_r f_0(\alpha - \Lambda_1)(\Phi_1 - \alpha\Phi_2)\,e^{i(\omega_1 + \omega_r)T_0}\\ &\quad\quad + A_2\alpha_1 m_r f_0(\alpha - \Lambda_2)(\Phi_1 - \alpha\Phi_2)\,e^{i(\omega_2 - \omega_r)T_0}\end{aligned}$$

$$
\begin{aligned}
&+ A_2\alpha_1 m_r f_0\,(\alpha-\Lambda_2)\,(\Phi_1-\alpha\Phi_2)\,e^{i(\omega_2+\omega_r)T_0}\\
&-\frac{1}{4}f_0^2\alpha_1 m_r(\Phi_1-\alpha\Phi_2)^2 e^{2i\omega_r T_0}\\
&- i\,(\Phi_1-\Phi_2\,\alpha)\,\beta\, f_0\omega_r\,\zeta\, e^{i\omega_r T_0}\\
&+ C.C. + CVF_1 \qquad (59)\\
&D_{0,0}\vartheta_1+\vartheta_1-k_r\alpha\,(\eta_1-\alpha\vartheta_1)\\
&=-2i\omega_1\left(D_1A_1+\sqrt{\frac{k_r}{m_r}}\zeta\alpha^2A_1\right.\\
&\left.+\kappa A_1-\sqrt{\frac{k_r}{m_r}}\zeta\alpha A_1\Lambda_1\right)e^{i\omega_1T_0}\\
&-2i\omega_2\left(D_1A_2+\sqrt{\frac{k_r}{m_r}}\zeta\alpha^2A_2\right.\\
&\left.+\kappa A_2-\sqrt{\frac{k_r}{m_r}}\zeta\alpha A_2\Lambda_2\right)e^{i\omega_2T_0}\\
&+{A_1}^2\left(\alpha_1\alpha(\alpha-\Lambda_1)^2-q_{zr}\right)e^{2i\omega_1T_0}\\
&+{A_2}^2\left(\alpha_1\alpha(\alpha-\Lambda_2)^2-q_{zr}\right)\\
&e^{2i\omega_2T_0}\\
&+2A_1\bar{A}_2\left(\alpha_1\alpha(\alpha-\Lambda_1)(\alpha-\bar{\Lambda}_2)-q_{zr}\right)\\
&e^{i(\omega_1-\omega_2)T_0}\\
&+2A_1A_2\,(\alpha_1\alpha(\alpha-\Lambda_1)(\alpha-\Lambda_2)-q_{zr})\\
&e^{i(\omega_1+\omega_2)T_0}\\
&-A_1f_0\,(\alpha_1\alpha\,(\alpha-\Lambda_1)\,(\Phi_1-\Phi_2\,\alpha)+\Phi_2q_{zr})\\
&e^{i(\omega_1-\omega_r)T_0}\\
&-A_1f_0\,(\alpha_1\alpha\,(\alpha-\Lambda_1)\,(\Phi_1-\Phi_2\,\alpha)+\Phi_2q_{zr})\\
&e^{i(\omega_1+\omega_r)T_0}\\
&-A_2f_0\,(\alpha_1\alpha\,(\alpha-\Lambda_2)\,(\Phi_1-\Phi_2\,\alpha)+\Phi_2q_{zr})\\
&e^{i(\omega_2-\omega_r)T_0}\\
&-A_2f_0\,(\alpha_1\alpha\,(\alpha-\Lambda_2)\,(\Phi_1-\Phi_2\,\alpha)+\Phi_2q_{zr})\\
&e^{i(\omega_2+\omega_r)T_0}\\
&+\frac{1}{4}f_0^2\left(\alpha_1\alpha(\Phi_1-\alpha\Phi_2)^2-q_{zr}\Phi_2^2\right)e^{2i\omega_rT_0}\\
&+i\left(-\Phi_2\kappa-\Phi_2\alpha^2\zeta\sqrt{\frac{k_r}{m_r}}\right.\\
&\left.+\alpha\zeta\sqrt{\frac{k_r}{m_r}}\Phi_1\right)f_0\,\omega_r e^{i\omega_rT_0}+C.C.+CVF_2
\end{aligned}
\qquad (60)
$$

Appendix D: superharmonic resonance near ω_1

$$
\begin{aligned}
\Gamma_1&=\frac{4\zeta l_1\beta\omega_1(\alpha-\Lambda_1)-4\alpha\sqrt{\frac{k_r}{m_r}}\zeta\omega_1(\alpha-\Lambda_1)-4\kappa\omega_1}{4\omega_1(1+l_1\Lambda_1)},\\
\Gamma_2&=\frac{-\alpha_1(\alpha-\Lambda_2)^2(l_1m_r-\alpha)-q_{zr}}{4\omega_1(1+l_1\Lambda_1)},\\
\Gamma_3&=\frac{-\alpha_1(\Phi_1-\alpha\Phi_2)^2(l_1m_r-\alpha)-q_{zr}\Phi_2^2}{4\omega_1(1+l_1\Lambda_1)},\\
\Gamma_4&=\frac{\alpha_1(\alpha-\bar{\Lambda}_2)(\alpha-\Lambda_1)(l_2m_r-\alpha)+q_{zr}}{2\omega_2(1+l_2\Lambda_2)},\\
\Gamma_5&=\frac{2\zeta l_2\beta\omega_2(\alpha-\Lambda_2)-2\alpha\sqrt{\frac{k_r}{m_r}}\zeta\omega_2(\alpha-\Lambda_2)-2\kappa\omega_2}{2\omega_1(1+l_2\Lambda_2)}.
\end{aligned}
\qquad (61)
$$

Appendix E: combined resonance

$$
\begin{aligned}
\Gamma_1&=\frac{-4\,\kappa\,\omega_1-4\,\alpha\,\zeta\sqrt{\frac{k_r}{m_r}}\omega_1\,(\alpha-\Lambda_1)+4\zeta l_1\,\beta\,\omega_1\,(\alpha-\Lambda_1)}{4\,\omega_1\,l_1\,\Lambda_1+4\,\omega_1}\\
\Gamma_2&=\frac{-\alpha_1(\alpha-\Lambda_2)^2(l_1m_r-\alpha)-q_{zr}}{4\omega_1(1+l_1\Lambda_1)}\\
\Gamma_3&=\frac{-2\,\alpha_1\,\left(\alpha-\bar{\Lambda}_2\right)(\alpha-l_1\,m_r)\,(\Phi_1-\Phi_2\,\alpha)-2\,q_{zr}\,\Phi_2}{4\omega_1(1+l_1\Lambda_1)}\\
\Gamma_4&=\frac{\alpha_1(\alpha-\bar{\Lambda}_2)(\alpha-\Lambda_1)(l_2m_r-\alpha)+q_{zr}}{2\omega_2(1+l_2\Lambda_2)}\\
\Gamma_5&=\frac{-\alpha_1\,\left(\alpha-\bar{\Lambda}_1\right)(\alpha-l_2\,m_r)\,(\Phi_1-\Phi_2\,\alpha)-q_{zr}\,\Phi_2}{2\omega_1(1+l_2\Lambda_2)}\\
\Gamma_6&=\frac{-2\,\alpha\,\zeta\sqrt{\frac{k_r}{m_r}}\,\omega_2\,(\alpha-\Lambda_2)+2\,\zeta\,\Lambda_2\,\beta\,\omega_2\,(\alpha-\Lambda_2)-2\,\kappa\,\omega_2}{2\,\omega_2+2\,\omega_2\,l_2\,\Lambda_2}
\end{aligned}
$$

Appendix F: linear stability of steady states

$$C_{44} = -\frac{f_0\Gamma_5\sin(\gamma_2^*)a_1^{*2} + \Gamma_3 f_0\sin(\gamma_2^*)a_2^{*2}}{a_2^* a_1^*}. \tag{69}$$

$$\mathbf{J}_{P1} = \begin{bmatrix} \Gamma_1 & 2\,\Gamma_2\sin(\gamma_1^*)\,a_2^* & \Gamma_2\cos(\gamma_1^*)\,a_2^{*2} & f_0\,\Gamma_3\cos(\gamma_2^*) \\ \Gamma_4\sin(\gamma_1^*)\,a_2^* & \Gamma_4\sin(\gamma_1^*)\,a_1^* + \Gamma_5 & \Gamma_4\cos(\gamma_1^*)\,a_2^*\,a_1^* & 0 \\ \frac{4\,\Gamma_4\cos(\gamma_1^*)\,a_1^* + \sigma_2}{a_1^*} & \frac{2\Gamma_2\cos(\gamma_1^*)\,a_2^*}{a_1^*} & \frac{-\Gamma_2\sin(\gamma_1^*)\,a_2^{*2} - 2\,\Gamma_4\sin(\gamma_1^*)\,a_1^{*2}}{a_1^*} & -\frac{f_0\,\Gamma_3\sin(\gamma_2^*}{a_1^*} \\ \frac{\sigma_1}{a_1^*} & \frac{2\Gamma_2\cos(\gamma_1^*)\,a_2^*}{a_1^*} & -\frac{\Gamma_2\sin(\gamma_1^*\,a_2^{*2}}{a_1^*} & -\frac{f_0\,\Gamma_3\sin(\gamma_1^*)}{a_1^*} \end{bmatrix}, \tag{62}$$

$$\mathbf{J}_{S1} = \begin{bmatrix} \Gamma_1 & 2\,\Gamma_2\sin(\gamma_1^*)\,a_2^* & \Gamma_2\cos(\gamma_1^*)\,a_2^{*2} & f_0^2\,\Gamma_3\cos(\gamma_2^*) \\ \Gamma_4\sin(\gamma_1^*)\,a_2^* & \Gamma_4\sin(\gamma_1^*)\,a_1^* + \Gamma_5 & \Gamma_4\cos(\gamma_1^*)\,a_2^*\,a_1^* & 0 \\ \frac{4\,\Gamma_4\cos(\gamma_1^*)\,a_1^* + \sigma_2}{a_1^*} & \frac{2\Gamma_2\cos(\gamma_1^*)\,a_2^*}{a_1^*} & \frac{-\Gamma_2\sin(\gamma_1^*)\,a_2^{*2} - 2\,\Gamma_4\sin(\gamma_1^*)\,a_1^{*2}}{a_1^*} & -\frac{f_0^2\,\Gamma_3\sin(\gamma_2^*}{a_1^*} \\ \frac{\sigma_1}{a_1^*} & \frac{2\Gamma_2\cos(\gamma_1^*)\,a_2^*}{a_1^*} & -\frac{\Gamma_2\sin(\gamma_1^*\,a_2^{*2}}{a_1^*} & -\frac{f_0^2\,\Gamma_3\sin(\gamma_1^*)}{a_1^*} \end{bmatrix}. \tag{63}$$

$$\mathbf{J}_{P2} = \tag{64}$$

$$\begin{bmatrix} \Gamma_1 & 2\Gamma_2\sin(\gamma_1^*)a_2^* & \Gamma_2\cos(\gamma_1^*)a_2^{*2} & 0 \\ \Gamma_4\sin(\gamma_1^*)a_2^* & \Gamma_5 + \Gamma_4 a_1^*\sin(\gamma_1^*) & \Gamma_4 a_1^*\cos(\gamma_1^*)a_2^* + f_0\Gamma_3\cos(\gamma_1^*) & 0 \\ \frac{-2f_0\Gamma_3\cos(\gamma_2^*)+4\Gamma_4 a_1^*\cos(\gamma_1^*)a_2^*+\sigma_2 a_2^*}{a_2^* a_1^*} & \frac{3\Gamma_2\cos(\gamma_1^*)a_2^{*2}+\sigma_2 a_1^*+2\Gamma_4 a_1^{*2}\cos(\gamma_1^*)}{a_2^* a_1^*} & \frac{-2\Gamma_4 a_1^{*2}\sin(\gamma_1^*)a_2^* - \Gamma_2\sin(\gamma_1^*)a_2^{*3}}{a_2^* a_1^*} & 2\frac{f_0\Gamma_3\sin(\gamma_2^*)}{a_2^*} \\ -\Gamma_4\cos(\gamma_1^*) & -\frac{-\sigma_1+\Gamma_4 a_1^*\cos(\gamma_1^*)}{a_2^*} & \Gamma_4 a_1^*\sin(\gamma_1^*) & -\frac{f_0\Gamma_3\sin(\gamma_2^*)}{a_2^*} \end{bmatrix} \tag{65}$$

$$\mathbf{J}_{S2} = \tag{66}$$

$$\begin{bmatrix} \Gamma_1 & 2\Gamma_2\sin(\gamma_1^*)a_2^* & \Gamma_2\cos(\gamma_1^*)a_2^{*2} & 0 \\ \Gamma_4\sin(\gamma_1^*)a_2^* & \Gamma_5 + \Gamma_4 a_1^*\sin(\gamma_1^*) & \Gamma_4 a_1^*\cos(\gamma_1^*)a_2^* + f_0{}^2\Gamma_3\cos(\gamma_1^*) & 0 \\ \frac{\sigma_2 a_2^* - 2f_0{}^2\Gamma_3\cos(\gamma_2^*)+4\Gamma_4 a_1^*\cos(\gamma_1^*)a_2^*}{a_2^* a_1^*} & \frac{2\Gamma_4 a_1^{*2}\cos(\gamma_1^*)+3\Gamma_2\cos(\gamma_1^*)a_2^{*2}+\sigma_2 a_1^*}{a_2^* a_1^*} & \frac{-\Gamma_2\sin(\gamma_1^*)a_2^{*3} - 2\Gamma_4 a_1^{*2}\sin(\gamma_1^*)a_2^*}{a_2^* a_1^*} & 2\frac{f_0{}^2\Gamma_3\sin(\gamma_2^*)}{a12} \\ -\Gamma_4\cos(\gamma_1^*) & -\frac{-\sigma_1+\Gamma_4 a_1^*\cos(\gamma_1^*)}{a_2^*} & \Gamma_4 a_1^*\sin(\gamma_1^*) & -\frac{f_0{}^2\Gamma_3\sin(\gamma_2^*)}{a_2^*} \end{bmatrix} \tag{67}$$

$$\mathbf{J}_C = \begin{bmatrix} C_{11} & C_{12} & C_{13} & C_{14} \\ C_{21} & C_{22} & C_{23} & C_{24} \\ C_{31} & C_{32} & C_{33} & C_{34} \\ C_{41} & C_{42} & C_{43} & C_{44} \end{bmatrix} \tag{68}$$

with

$$C_{11} = \Gamma_1,\ C_{12} = \Gamma_3 f_0\sin(\gamma_2^*) + 2\Gamma_2\sin(\gamma_1^*)a_2^*,$$

$$C_{13} = \Gamma_2\cos(\gamma_1^*)a_2^{*2},\ C_{14} = \Gamma_3 f_0\cos(\gamma_2^*)a_2^*,$$

$$C_{21} = \Gamma_4\sin(\gamma_1^*)a_2^* + f_0\Gamma_5\sin(\gamma_2^*),$$

$$C_{22} = \Gamma_6 + \Gamma_4\sin(\gamma_1^*)a_1^*,$$

$$C_{23} = \Gamma_4\cos(\gamma_1^*)a_2^*a_1^*,\ C_{24} = f_0\Gamma_5\cos(\gamma_2^*)a_1^*,$$

$$C_{31} = \frac{4\Gamma_4\cos(\gamma_1^*)a_2^*a_1^* - 4f_0\Gamma_5\cos(\gamma_2^*)a_1^* + \sigma_2 a_2^*}{a_2^*a_1^*},$$

$$C_{32} = \frac{3\Gamma_2\cos(\gamma_1^*)a_2^{*2} + \sigma_2 a_1^* + 2\Gamma_4\cos(\gamma_1^*)a_1^{*2} + 2\Gamma_3 f_0\cos(\gamma_2^*)a_2^*}{a_2^*a_1^*},$$

$$C_{33} = \frac{-2\Gamma_4\sin(\gamma_1^*)a_1^{*2}a_2^* - \Gamma_2\sin(\gamma_1^*)a_2^{*3}}{a_2^*a_1^*},$$

$$C_{34} = \frac{2f_0\Gamma_5\sin(\gamma_2^*)a_1^{*2} - \Gamma_3 f_0\sin(\gamma_2^*)a_2^{*2}}{a_2^*a_1^*}$$

$$C_{41} = -\frac{-2f_0\Gamma_5\cos(\gamma_2^*)a_1^* - \sigma_1 a_2^* + 2\Gamma_4\cos(\gamma_1^*)a_2^*a_1^*}{a_2^*a_1^*},$$

$$C_{42} = -\frac{-3\Gamma_2\cos(\gamma_1^*)a_2^{*2} + \Gamma_4\cos(\gamma_1^*)a_1^{*2} - \sigma_1 a_1^* - 2\Gamma_3 f_0\cos(\gamma_2^*)a_2^*}{a_2^*a_1^*},$$

$$C_{43} = -\frac{-\Gamma_4\sin(\gamma_1^*)a_1^{*2}a_2^* + \Gamma_2\sin(\gamma_1^*)a_2^{*3}}{a_2^*a_1^*},$$

References

1. Alting, L., Kimura, F., Hansen, H.N., Bissacco, G.: Micro engineering. CIRP Ann.-Manuf. Technol. **52**(2), 635–657 (2003)
2. Hansen, H.N., Carneiro, K., Haitjema, H., De Chiffre, L.: Dimensional micro and nano metrology. CIRP Ann. **55**(2), 721–743 (2006)
3. Ehmann, K.F.: A Synopsis of us Micro-Manufacturing Research and Development Activities and Trends, pp. 7–13. Borovets, Bulgaria (2007)
4. Karnopp, D.: Active and semi-active vibration isolation. In: Elarabi, M.E., Wifi, A.S., Wifi, A.S. (eds.) Current Advances in Mechanical Design and Production VI, pp. 409–423. Elsevier (1995)
5. Schellekens, P., Rosielle, N., Vermeulen, H., Vermeulen, M.M.P.A., Wetzels, S.F.C.L., Pril, W.: Design for precision: current status and trends. CIRP Ann. **47**(2), 557–586 (1998)
6. Liu, Y., Waters, T.P., Brennan, M.J.: A comparison of semi-active damping control strategies for vibration isolation of harmonic disturbances. J. Sound Vib. **280**(1–2), 21–39 (2005)
7. Fuller, C.C., Elliott, S., Nelson, P.A.: Active Control of Vibration. Academic Press, USA (1996)

8. Shiba, K., Mase, S., Yabe, Y., Tamura, K.: Active/passive vibration control systems for tall buildings. Smart Mater. Struct. **7**(5), 588 (1998)
9. Jalili, N.: A comparative study and analysis of semi-active vibration-control systems. J. Vib. Acoust. **124**(4), 593–605 (2002)
10. DeBra, D.B.: Vibration isolation of precision machine tools and instruments. CIRP Ann.-Manuf. Technol. **41**(2), 711–718 (1992)
11. Rivin, E.I.: Vibration isolation of precision equipment. Precis. Eng. **17**(1), 41–56 (1995)
12. Franchek, M.A., Ryan, M.W., Bernhard, R.J.: Adaptive passive vibration control. J. Sound Vib. **189**(5), 565–585 (1996)
13. Weaver Jr., W., Timoshenko, S.P., Young, D.H.: Vibration Problems in Engineering. Wiley, New York (1990)
14. Harris, C.M., Piersol, A.G.: Harris' Shock and Vibration Handbook, vol. 5. McGraw-Hill, New York (2002)
15. Rivin, E.I.: Passive Vibration Isolation. American Society of Mechanical, (2003)
16. Crede, C.E.: Vibration and Shock Isolation. Wiley, New York (1951)
17. Snowdon, J.C.: Vibration and Shock in Damped Mechanical Systems. Wiley, New York (1968)
18. Snowdon, J.C.: Vibration isolation: use and characterization. J. Acoust. Soc. Am. **66**(5), 1245–1274 (1979)
19. Ryaboy, V.M.: Static and dynamic stability of pneumatic vibration isolators and systems of isolators. J. Sound Vib. **333**(1), 31–51 (2014)
20. Subrahmanyan, P.K., Trumper, D.L.: Synthesis of passive vibration isolation mounts for machine tools-a control systems paradigm. In: American Control Conference, 2000. Proceedings of the 2000, vol. 4, pp. 2886–2891. IEEE (2000)
21. Rivin, E.I.: Vibration isolation of precision objects. Sound Vib. **40**(7), 12–20 (2006)
22. Okwudire, C.E.: A study on the effects of isolator, motor and work surface heights on the vibrations of ultra-precision machine tools, In: Proceeding of ICOMM, Evanston, Illinois, pp. 31–36, March (2012)
23. Shin, Y.-H., Kim, K.-J., Chang, P.-H., Han, D.K.: Three degrees of freedom active control of pneumatic vibration isolation table by pneumatic and time delay control technique. J. Vib. Acoust. **132**(5), 051013 (2010)
24. Vermeulen, M.M.P.A., Rosielle, P.C.J.N., Schellekens, P.H.J.: Design of a high-precision 3d-coordinate measuring machine. CIRP Ann.-Manuf. Technol. **47**(1), 447–450 (1998)
25. Kato, T., Kawashima, K., Sawamoto, K., Kagawa, T.: Active control of a pneumatic isolation table using model following control and a pressure differentiator. Precis. Eng. **31**(3), 269–275 (2007)
26. Erin, C., Wilson, B., Zapfe, J.: An improved model of a pneumatic vibration isolator: theory and experiment. J. Sound Vib. **218**(1), 81–101 (1998)
27. Bukhari, M., Barry, O: On the nonlinear vibration analysis of ultra precision manufacturing machines with mode coupling. In: ASME 2017 International Design Engineering Technical Conferences and Computers and Information in Engineering Conference (2017)
28. Kirk, C.L.: Non-linear random vibration isolators. J. Sound Vib. **124**(1), 157–182 (1988)
29. Ruzicka, J.E., Derby, T.F.: Influence of damping in vibration isolation. Technical Report (1971)
30. Ibrahim, R.A.: Recent advances in nonlinear passive vibration isolators. J. Sound Vib. **314**(3–5), 371–452 (2008)
31. Ewins, D.J., Rao, S.S., Braun, S.G.: Encyclopedia of Vibration, Three-Volume Set. Academic Press, USA (2002)
32. Racca Sr, R: How to select power-train isolators for good performance and long service life. SAE Transactions, pp. 3439–3450 (1982)
33. Andrews, F.: Items which can compromise vibration isolation (2012)
34. Okwudire, C.E., Lee, J.: Minimization of the residual vibrations of ultra-precision manufacturing machines via optimal placement of vibration isolators. Precis. Eng. **37**(2), 425–432 (2013)
35. Lee, J., Okwudire, C.E.: Reduction of vibrations of passively-isolated ultra-precision manufacturing machines using mode coupling. Precis. Eng. **43**, 164–177 (2016)
36. Natsiavas, S., Tratskas, P.: On vibration isolation of mechanical systems with non-linear foundations. J. Sound Vib. **194**(2), 173–185 (1996)
37. Nayfeh, A.H., Mook, D.T., Marshall, L.R.: Nonlinear coupling of pitch and roll modes in ship motions. J. Hydronaut. **7**(4), 145–152 (1973)
38. Karabalin, R.B., Cross, M.C., Roukes, M.L.: Nonlinear dynamics and chaos in two coupled nanomechanical resonators. Phys. Rev. B **79**(16), 165309 (2009)
39. Mathis, A.T., Quinn, D.D.: Transient dynamics, damping, and mode coupling of nonlinear systems with internal resonances. Nonlinear Dyn. **99**(1), 269–281 (2020)
40. Rocha, R.T., Balthazar, J.M., Quinn, D.D., Tusset, A.M., Felix, J.L.P.: Non-ideal system with quadratic nonlinearities containing a two-to-one internal resonance. In: ASME 2016 International Design Engineering Technical Conferences and Computers and Information in Engineering Conference. American Society of Mechanical Engineers Digital Collection (2016)
41. Krifa, M., Bouhaddi, N., Chevallier, G., Cogan, S., Kacem, N.: Estimation and correction of the modal damping error involving linear and nonlinear localized dissipation. Eur. J. Mech.-A/Solids **66**, 296–308 (2017)
42. Heertjes, M., van de Wouw, N.: Nonlinear dynamics and control of a pneumatic vibration isolator. J. Vib. Acoust. **128**(4), 439–448 (2006)
43. Nayfeh, A.H., Mook, D.T.: Nonlinear Oscillations. Wiley, New York (2008)
44. Balachandran, B., Nayfeh, A.H.: Cyclic motions near a hopf bifurcation of a four-dimensional system. Nonlinear Dyn. **3**(1), 19–39 (1992)
45. Poole, E., Roberson, B., Stephenson, B.: Weak allee effect, grazing, and s-shaped bifurcation curves. Involv. J. Math. **5**(2), 133–158 (2013)